High Sensitive and High Resolution Refractive Index Sensor using Critically Coupled Silicon Micro-ring Resonator

A Project Report

submitted by

SOORAJ M S

in partial fulfillment of the requirements
for the award of the degree of

MASTER OF TECHNOLOGY

DEPARTMENT OF ELECTRICAL ENGINEERING
INDIAN INSTITUTE OF TECHNOLOGY MADRAS.

May 2017

THESIS CERTIFICATE

This is to certify that the thesis titled **High sensitive and high resolution refractive index sensor using critically coupled silicon micro-ring resonator** , submitted by **Sooraj M S** bearing Roll number **EE15M058**, to the Indian Institute of Technology, Madras, for the award of the degree of **Master of Technology**, is a bona fide record of the research work done by him under our supervision. The contents of this thesis, in full or in parts, have not been submitted to any other Institute or University for the award of any degree or diploma.

Dr. Bijoy Krishna Das
Project Guide
Associate Professor
Dept. of Electrical Engineering
IIT-Madras, 600 036

Place: Chennai, India

Date: Fri 16th Jun, 2017

Dedicated to my Parents and Friends...

ACKNOWLEDGEMENTS

First of all, I would like to sincerely thank my guide Dr. Bijoy krishna Das for his valuable technical guidance as well as for the much needed encouragement and support. It has been a great opportunity working under him and this work would not have been possible if not for his vast expertise in the area of Opto-electronics.

I am very thankful to each and every member of the Integrated Optoelectronics group for their valuable support during the course of my work. Their support and immense knowledge in Silicon Photonics helped me for the successful completion of the thesis. I would like to thank all the members of the MEMS lab where i have done my fabrication for their help and support during the project.

Special thanks to Sujith Chandran and Ramesh K for rendering their help and support. I am very grateful to them for teaching and training me the simulation as well as fabrication processes and for helping me in various fabrication and characterization steps. I express my sincere gratitude to Sumi R, Sreevatsa Kurudi, Riddhi Nandi, Amrutha N, Keerthana Murugan, Srinath Jagan, Parimal Sah and Arijith Misra who are the members of Integrated Optoelectronics team for giving good motivation and suggestions in the group discussions and also helping me in various stages of my project work.

I would like to thank the Department of Electrical Engineering, IIT Madras for offering the most comprehensive curriculum, and for encouraging the students to work in an area of their interest. I would like to thank the Head of the Department [write your hod name here] and all the faculty members of the department. Last but not the least, I would also like to thank my friends and family members for their continued support during the course of this work.

ABSTRACT

Various parameters which affects the sensitivity and limit of detection of a critically coupled ring resonator refractive index sensor has been studied using computer simulations and modeling. Simulation results point out to the fact that the sensitivity strongly depends on directional coupler dimensions and we have optimized the parameters of the same for better sensitivity. The role of ring dimensions on the limit of detection of the sensor device was also analyzed.

Simulation results shows that deeply etched directional couplers with larger width waveguides spaced close to each other can interact with the cladding refractive index more effectively. The calculated sensitivity of a deeply etched (25 nm slab) is about 260 nm/RIU. The limit of detection of the device can be improved by reducing the FSR of the ring by increasing the perimeter of the ring. We could show that a ring of 7 mm perimeter can give limit of detection less than 10^{-4} RIU.

The compact structure for the proposed ring resonator sensor and a compact mask file for the same have been designed. The spin coating system is optimized for thicker HSQ coatings for deep etching and the selectivity and etching rate of Silicon and HSQ in ICPRIE etching have been studied. The observed sensitivity of the device after 90 nm etching is 95 nm/RIU and the FSR of the 7 mm ring is about 80 pm. The Q-factors of the resonators increases with ring perimeter and the maximum value obtained is 61000 for a ring of 7.195 mm perimeter. The superiority of the proposed integrated optical sensor device lies in its high sensitivity, high Limit of detection, simpler design, easier operation, wider-range of uniform sensitivity.

TABLE OF CONTENTS

LIST OF FIGURES

ABBREVIATIONS

Acronyms

CMOS	Complementry Metal Oxide Semiconductor
DI	De-ionized (water)
FSR	Free Spectral Range
ICP	Inductively Coupled Plasma
PPR	Positive Photo Resist
LOD	Limit of Detection
RIE	Reactive Ion Etching
SEM	Scanning Electron Microscope
SMF	Single Mode Fiber
SOI	Silicon-On-Insulator
TE	Transverse Electric (polarization)
TM	Transverse Magnetic (polarization)

Units

dB	decibel
dBm	decibel milli-watt
mW	milli watt
μW	micro watt
μm	micrometer
ns	nano Second
μs	micro second
pm	pico meter

NOTATIONS

$\mathbf{n}$	Refractive index
$\mathbf{n}_{eff}$	Effective refractive index
$\boldsymbol{\epsilon}$	Permitivity
$\boldsymbol{\lambda}$	Wavelength
$\boldsymbol{\beta}$	Propagation constant
$\boldsymbol{\phi}$	Phase of the EM wave
$\mathbf{L}$	Length (refers to device length, component length)
$\boldsymbol{\Gamma}$	Overlap integral coefficient
$\boldsymbol{\alpha}$	Loss per unit length

CHAPTER 1

Introduction

1.1 Electronics and Photonics

Electronics plays a major role in our day to day life and different areas of science and technologies like Telecommunications, High speed computing, Instrumentation, Biomedical and Sensing. Invention of integrated chips(IC) marked the evolution of electronics. The development of compact and high speed devices could be attributed to the invention of ICs. The development of CMOS fabrication technology lead to the phenomenal development in electronics industry. The need for high speed and compact devices increased gradually and the density of transistors also increased exponentially. As the transistor size is scaling down, its speed and integration density is following Moore's law [1]. But, the interconnect delay is significantly higher when the metal interconnects from device to device or chip to chip are scaled down to submicron regime. At higher operating frequencies, the down scaled metal lines exhibit higher resistance and capacitance which in turn increases the RC time delay; resulting into an over-all limitation in microprocessor speed and the bandwidth. And the power dissipation is also exponentially increased.

It is identified that the interconnect delay can be reduced by replacing electronic interconnects by optical interconnects. Optical interconnects can increase the speed as well as the bandwidth of the devices. Compatibility with existing CMOS fabrication technology, energy efficiency, high speed optoelectronics conversion and higher integration density are the basic requirements for an optical interconnect. These demands push towards to a default solution to use Silicon for photonics circuits too. Since the bandgap of Silicon is $1.12eV$, it is transparent to the IR and MIR wavelengths which are used for optical communication. Another advantage of silicon (with air or SiO_2 as cladding) is its high refractive index contrast which will help us to integrate compact

photonics circuits within a chip. It can be integrated with electronics in the same device layer using the same process flow as for CMOS electronics.

1.2 Silicon Photonics and Bio-sensing

The success of CMOS compatible Silicon photonics has led to the development of photonics circuits integrated with electronics and Lab-on-Chip in SOI for different type of sensing applications. Sensing the refractive index of the material is the key for most sensing applications and many devices and mechanisms for the same has been demonstrated in SOI platform. Micro ring resonator, Photonic crystals, Mach-Zehnder interferometer, Distributed Bragg Reflectors (DBR) and Young's interferometer are some examples. Among these, the micro ring resonators are very sensitive to cladding refractive index and they can be designed to get large interaction length with the analyte [2] [3].

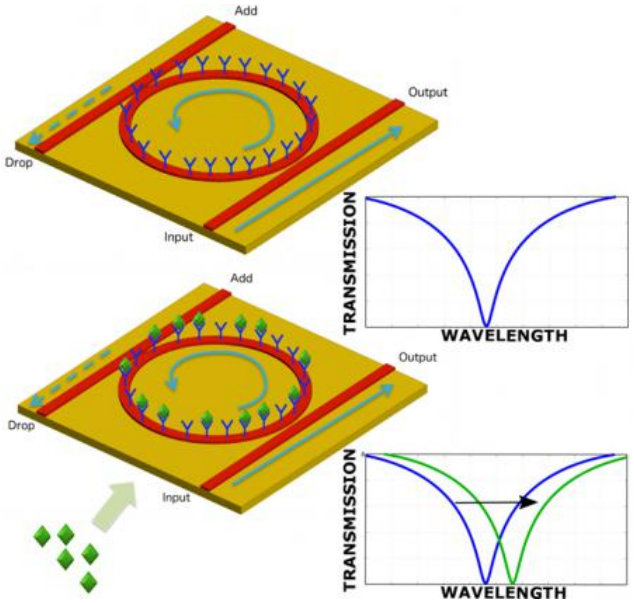

Figure 1.1: Bio-sensing technique using micro-ring resonator

1.3 Literature Review and Motivation

The important parameters which describe the quality of a sensor are the sensitivity (S) and the limit of detection (LOD). In ring resonator based sensors, the sensing is mainly performed by measuring the shift of a given order of resonance wavelength. Therefore, sensitivity is defined as the shift in resonance wavelength per refractive index unit (RIU). The LOD is given by $\frac{\lambda_m}{QS}$, where λ_m is the given mth order of resonant wavelength, Q is the quality factor for λ_m and S is the sensitivity . The value of S can be increased by increasing the interaction of field with the analyte. LOD mainly depends on Sensitivity and Q factor. Q factor is a measure of capacity of a resonator to store the energy and it can be increased by decreasing the waveguide loss and resonator volume. In the case of a ring resonator, the interaction with the analyte is not estimated using the physical length of the resonator but with number of revolutions inside the ring and which would be indicated by the quality factor (Q-factor) of the resonator. The effective length (L_{eff}) of a ring resonator can be related to its Q-factor as,

$$L_{eff} = Q\frac{\lambda_m}{2\pi n_{eff}} \tag{1.1}$$

Where n_{eff} is the effective index of the guided mode in the waveguide. the Q-factor is defined as,

$$Q - factor = \frac{\lambda_m}{FWHM} \tag{1.2}$$

Where FWHM is the Full Width Half Maximum of the resonant wavelength. Silicon ring resonators of Q-factor 10^6 with a ring perimeter of length 50 -100 μm is equivalent to a straight waveguide of 10 cm long.

In general, Sensitivity is limited by the evanescent field overlap with the cladding material of a conventional waveguide ring resonator. Rodriguez et al. could enhance the light matter interaction by fabricating the ring resonator with porous silicon waveguides and reported an improved value of sensitivity (380 nm/RIU). But porous silicon will increase the waveguide loss and hence the quality factor is low (10 000)[6]. Recently one group showed that the value of S could be increased to record value 24 300 nm/RIU

by making use of Vernier effect of cascaded ring resonators. The sensitivity value is attractive in this case, but they are complex in terms of device design and operation[7].

Another type of sensor design is slot waveguide type in which the guided mode will be between the waveguide gap of a directional coupler. This type of ring resonator was found attractive because of direct interaction of analytes with the guided mode which is mostly in the cladding region. Recently, a ring resonator designed with slot waveguides has been shown to be highly sensitive (1300 nm/RIU). Since the guided mode is mostly in the waveguide region the loss is very high and it can be designed for only shallow range of refractive indices of analytes[8].

Recently, Sujith Chandran et al. have designed and demonstrated a wide range refractive index sensor based on critically coupled silicon micro-ring resonator with average sensitivity of 57 nm/RIU and LOD of 1.6×10^{-2} RIU.

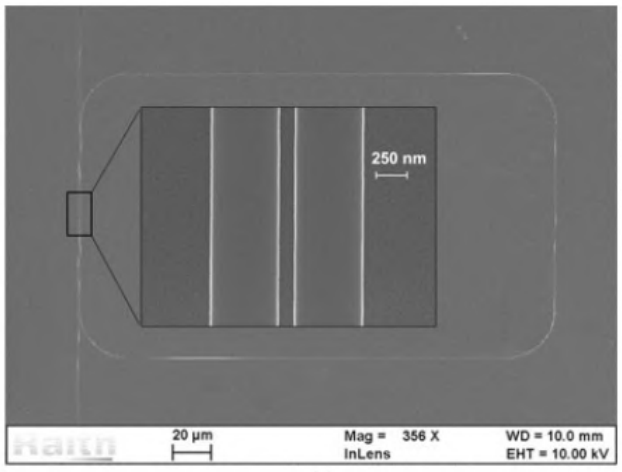

Figure 1.2: SEM image of typical micro-ring resonator fabricated on SOI

The SEM image of the fabricated device and output spectra recorded for three different cladding refractive indices are given in Figures 1.2 and 1.3. The device is fabricated in 250 nm device layer SOI platform using rib waveguides. The waveguides and directional couplers where shallow etched (about 100 nm) keeping a slab height of 150 nm. Simpler design, easier operation and wide range of uniform sensitivity are the main advantages of this type of sensor design [4].

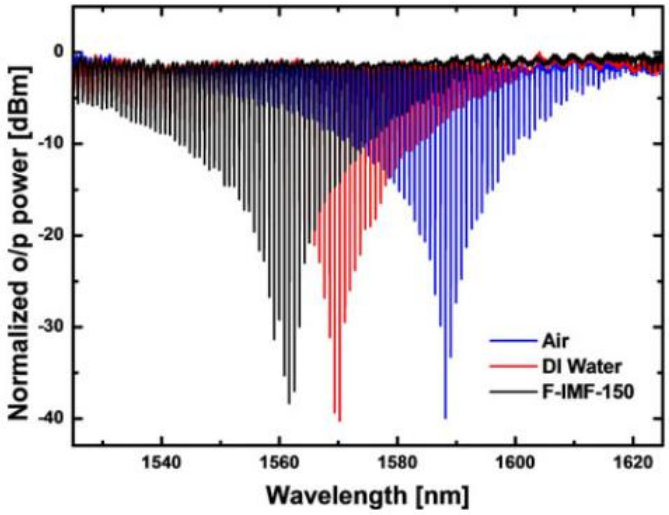

Figure 1.3: Output spectra for different background indices

1.4 Research Objective

The key objective of my work is to enhance the sensitivity and LOD of the critically coupled miro-ring resonator. The sensitivity of the device can be increased by increasing the interaction of analyte with the evanacent field of the guided mode. Another important parameter that determines the performance of a sensor is the limit of detection (LOD). LOD strongly depends on the Free Spectral Range (FSR), Q-factor of the resonator and Sensitivity. Hence my work focuses on design and fabrication of a compact high sensitive device with improved limit of detection.

1.5 Thesis Organization

The thesis is organized in four chapters. First chapter gives an introduction to Silicon Photonics and bio-sensing. It also discusses various ongoing research works in this field and motivation that lead to do this research. The second chapter discusses the theoretical background of various components which will be used in our sensor design. The simulation results and fabrication followed by the characterization results are discussed in the third chapter. In the final chapter, the summary of the project and outlook has been discussed in brief.

CHAPTER 2

Background Theory

2.1 Single-mode Waveguides

The pivotal thing that affects the design of photonic devices is the type of wave guides which in turn vary from applications to applications. Hence it is important to make sure that whether your device need single-mode waveguides or multi-mode waveguides. For most of the applications we have been using single-mode waveguides to avoid complexity in operation.

Single-mode waveguides (assumed for operating wavelength λ 1550 nm) are preferred since the loss and inter-modal dispersion are minimal. Though the typical length of waveguides used in integrated optics and/or on-chip optical interconnect devices is much smaller than the optical fibers used for long-haul and/or short-haul communication systems, inter modal dispersion plays a vital role at high speed optical interconnect devices. Particularly in resonant structures such as ring resonators, Fabry-Perot cavities, the existence of higher order modes makes additional resonant peaks which is undesirable. Thus, single-mode guidance is a necessary condition for most of integrated optical functions. Sujith Chandran et al studied the behavior of waveguides in SOI for different dimensions and found the single-mode cut off for 250 nm device layer SOI platform and is given in figure 2.1

The calculations are for Transverse Electric (TE) polarization and from the plot we can see that the waveguides are single-mode below the width about 550 nm for a slab height of 25 nm.

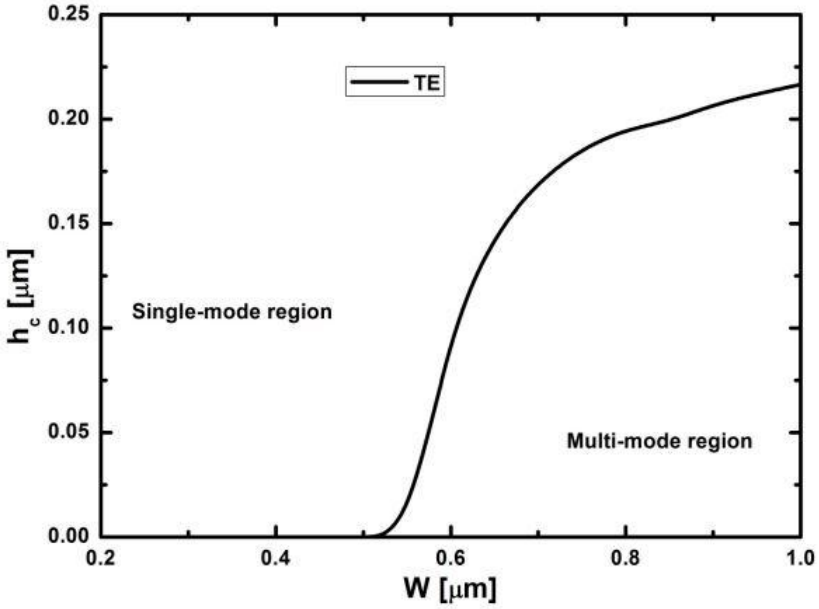

Figure 2.1: Single-mode and Muti-mode cut off regions for a 250 nm device layer

2.2 Directional coupler

Before entering to the discussion about micro ring resonators, we can discuss some basics of light coupling between waveguides. Two single-mode waveguides placed adjacent to each other as shown in the figure 2.2 is called directional coupler. If we couple light into the input of one of the waveguides, it will start to propagate and couple back and forth between both the waveguides in the directional coupler region.

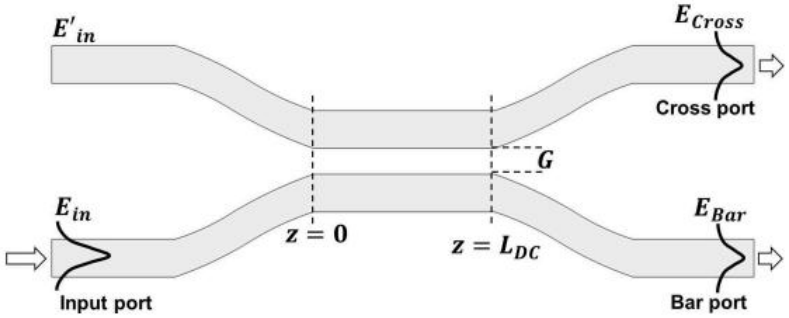

Figure 2.2: Directional Coupler

The modes supported by the two waveguide system can be expressed as one symmetric mode and one anti-symmetric mode as given in figure 2.3.

Since the effective index for the symmetric and anti-symmetric modes are different,

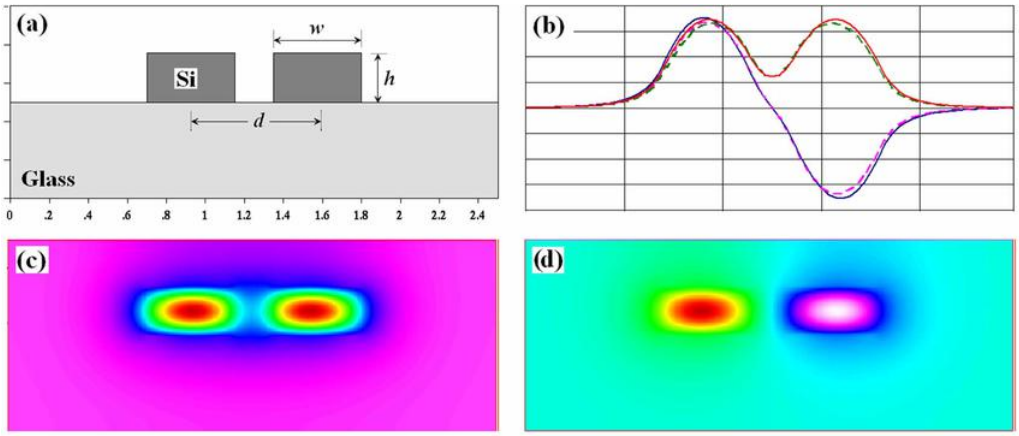

Figure 2.3: Directional Coupler : (a) Cross sectional view, (b) Symmetric and Anti-symmetric modes, (c) and (d) are mode profiles of Symmetric and Anti-symmetric modes

there will be some phase shift between the modes as the light propagates through it. So, the intensity of light in any waveguide in a directional coupler will be a super position of these two modes. For a phase difference of 180° between the symmetric and anti-symmetric modes, both modes will interfere constructively in the second waveguide and destructively interfere in the first waveguide, and the total power will be in the 2nd waveguide.

The directional coupler length for total power coupling to the 2nd waveguide is given by,

$$L_c = \frac{\lambda_m}{2\Delta n} \tag{2.1}$$

Where Δn is the difference between the effective indices of symmetric and anti-symmetric modes. This distance of total power coupling to the second waveguide is called cross coupling length (Lc). It will vary for different dimensions of directional coupler. The power coupling between the two waveguides in a directional coupler is graphically represented in Fig 2.4

2.3 Ring Resonator

A ring resonator is nothing but directional coupler in which the output of one of the arm is feedback to the input of the same arm as given in the figure. So, the second arm will form a close loop. The ring will be resonant for certain wavelengths for which the total

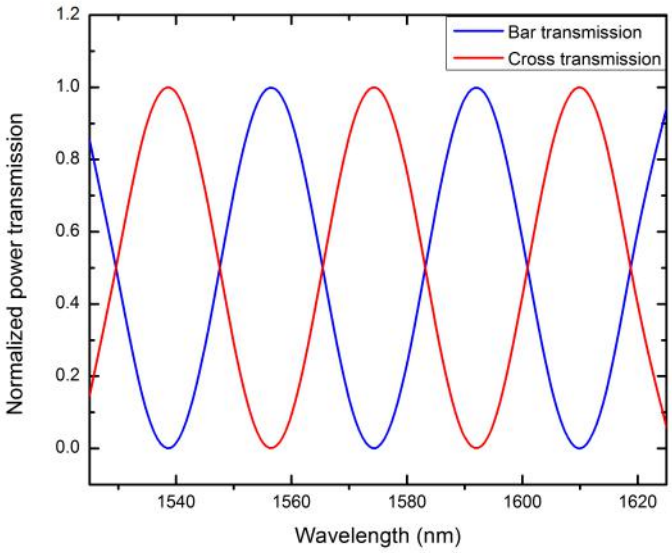

Figure 2.4: Power variation in bar and cross ports of a directional coupler

optical path length of the ring matches with the integer multiple of the wavelength.

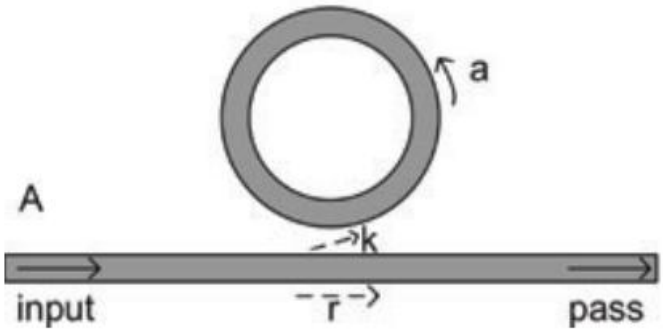

Figure 2.5: Ring resonator

2.3.1 All-pass filter (APF) configuration

An all-pass filter (APF) is the simplest form of ring resonator in which one of the arms of a directional coupler is feedback to the input as given in the Figure 2.5. The ratio between transmitted and incident field in the bus waveguide is given by,

$$\frac{E_{pass}}{E_{input}} = e^{i(\pi+\phi)} \frac{a - re^{-i\phi}}{1 - rae^{i\phi}} \tag{2.2}$$

Where $\phi = \beta L$ is the single-pass phase shift, with L the round trip length and β is the propagation constant of the circulating mode. a is the single-pass amplitude transmission, including both propagation loss in the ring and loss in the couplers. It relates to the power attenuation coefficient α [1/cm] as $a^2 = \exp(-\alpha L)$. The term r in the equation is the self coupling coefficient of the directional coupler.

By squaring the field equation, we will get the intensity transmission as

$$T_n = \frac{I_{pass}}{I_{input}} = \frac{a^2 - 2racos\phi + r^2}{1 - 2racos\phi + (ra)^2} \tag{2.3}$$

Where all the symbols have usual meaning . Similarly, we can define k as the cross-coupling coefficients, and so r^2 and k^2 are the power splitting ratios of the coupler, and they are assumed to satisfy $r^2 + k^2 = 1$, assuming there are no losses in the coupling section. We find the ring to be on resonance when the phase ϕ is a multiple of 2π, or when the wavelength of the light fits a whole number of times inside the optical length of the ring[4].

$$\lambda_{res} = \frac{n_{eff}L}{m} \quad \text{where} \quad m = 1, 2, 3, ... \tag{2.4}$$

From the intensity transmission equation we can observe that the extinction ratio of the resonant wavelength will depend on the loss factor a of the ring for that specific wavelength. For a resonant wavelength if loss factor inside the ring is equal to the amplitude transmission factor r of the directional coupler region, then both the waves from the ring and from the input of the directional coupler will interfere destructively to make the output intensity zero for that particular wavelength. Ie. When $a = r$ $T_n = 0$. This condition is called critical coupling for which we will get maximum extinction for a particular wavelength. If the optical losses in the waveguide ring and DC remain constant within the wavelength range of detection, the critically coupled resonant wavelength is given by,

$$\lambda_c = \frac{\pi L_{dc} \Delta n(\lambda_c)}{sin^{-1}(k_c)} \tag{2.5}$$

Where k_c is the cross coupling coefficient for critically coupled wavelength, L_{dc} is the directional coupler length and Δn is the difference in n_{eff} for the symmetric and

anti-symmetric modes of the directional coupler. Wavelength dependent cross coupling coefficient is given by,

$$k(\lambda) = sin\Big[\frac{\pi \Delta n(\lambda) L_{dc}}{\lambda}\Big] \tag{2.6}$$

The shift in critically coupled resonance wavelength because of differential change in cladding refractive index can be derived as

$$\Delta\lambda_c = -\frac{\lambda_c}{\Delta n_g(\lambda_c)}\Big(\frac{d\Delta n}{dn_c}\Big)_{\lambda=\lambda_c}\Delta n_c \tag{2.7}$$

where

$$\Delta n_g = \lambda\frac{d\Delta n(\lambda)}{d\lambda} - \Delta n(\lambda) \tag{2.8}$$

Where n_c is the cladding refractive index, n_g is called the group index of the directional coupler region for a given wavelength and the Δn_g is the differential change in group index. $\Delta\lambda_c$ is the shift in critically coupled resonant wavelength for a change of Δn RIU.

2.3.2 Add-Drop configuration

There is another ring resonator configuration which is used widely in many applications. If we place another waveguide in the other side of the ring, it is called add-drop configuration as given in Figure 2.6. The transmission at pass and drop port are given by,

$$T_p = \frac{I_{pass}}{I_{input}} = \frac{r_2^2a^2 - 2r_1r_2acos\phi + r_1^2}{1 - 2r_1r_2acos\phi + (r_1r_2a)^2} \tag{2.9}$$

$$T_d = \frac{I_{drop}}{I_{input}} = \frac{(1-r_1^2)(1-r_2^2)a}{1 - 2r_1r_2acos\phi + (r_1r_2a)^2} \tag{2.10}$$

Where $a^2 = e^{-(\alpha L)}$ is the loss factor and α is the loss coefficient. Here $\phi = \frac{2\pi}{\lambda}n_{eff}L$. Where L is the perimeter of the ring and n_{eff} is the effective index of the guided mode in

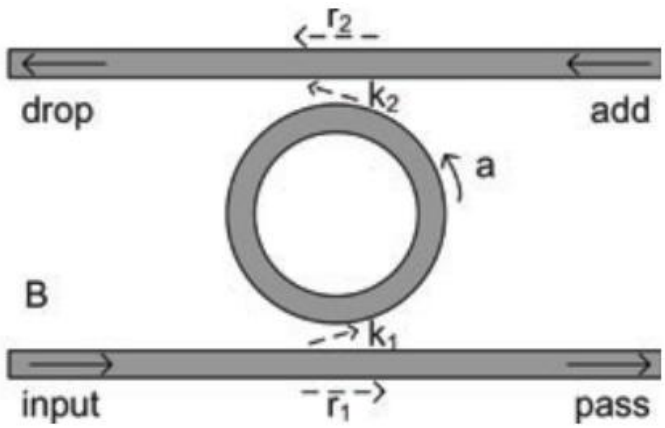

Figure 2.6: Ring resonator: Add- Drop configuration

the waveguide. In this type of add-drop configuration, we can add and drop wavelengths modulated with different information using the second waveguide containing drop port and is very useful in different communication related applications[10].

2.4 Grating Coupler

Coupling light into the integrated chip from the fiber and coupling back to fiber from the output of the integrated device is very important in integrated photonic related applications. Grating coupler is a component used for coupling light from fiber to waveguide without physical contact. It is a periodic dielectric grating structure which is designed to couple a band of wavelength efficiently.The schematic representation of the grating coupler structure in SOI is given in Figure 2.7.

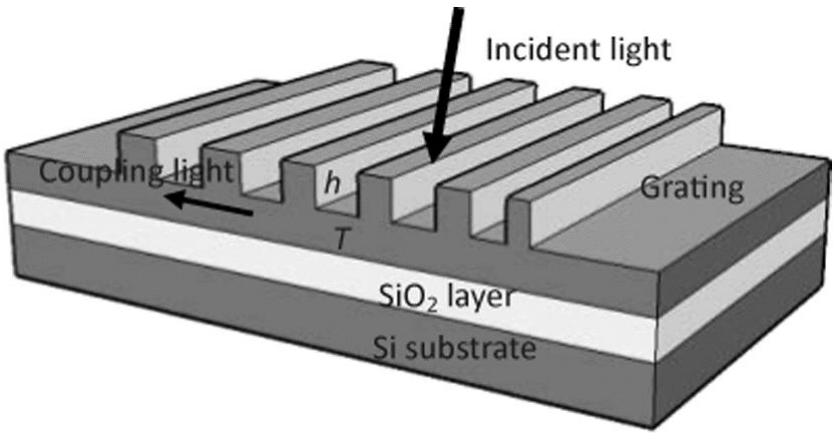

Figure 2.7: Grating coupler

The period required for the grating for coupling a particular wavelength λ_0 is given by,

$$\Lambda = m\frac{\lambda_0}{n_{eff} - n_0 sin(\theta)} \tag{2.11}$$

Where n_{eff} is the effective index of grating region. n_0 is the refractive index of background media and θ is the angle between fiber and the grating.

CHAPTER 3

Results and Discussion

3.1 Simulation results

The simulations for this project work is mostly done in Lumerical Mode solver and Matlab. The study related to waveguides, directional coupler and grating coupler are done in Lumerical Mode Solver and results related to ring resonator is obtained by modeling in Matlab. The plots are generated using both the Matlab and OriginPro.

3.1.1 Directional coupler dimensions and Sensitivity

As we have seen in previous chapters, light coupling between waveguides in a directional coupler and confinement of light in the waveguide are very crucial for sensing applications. The interaction of light with the background material is also very important. All these parameters can be controlled by proper designing of directional coupler and waveguide dimensions.The simulated mode profiles for a directional coupler modes for two different dimensions are given in Fig 3.1

Figure 3.1 (a) and (b) represents the symmetric and anti-symmetric mode profiles for a shallow etched directional coupler. We can see that the confinement is poor in this case but the coupling between waveguides is very high. In this case the power transfer between the waveguides will be much faster and it will be mostly through the slab region. So the dependence of background refractive in power coupling will be very less in this case. One advantage of the shallow etched directional coupler is the short cross coupling length.

The mode profiles for a fully etched directional coupler is given in figure 3.1 (c) and (d). The optical modes are highly confined and the power coupling between the waveguides is happening mostly through the coupler gap region. So the interaction between

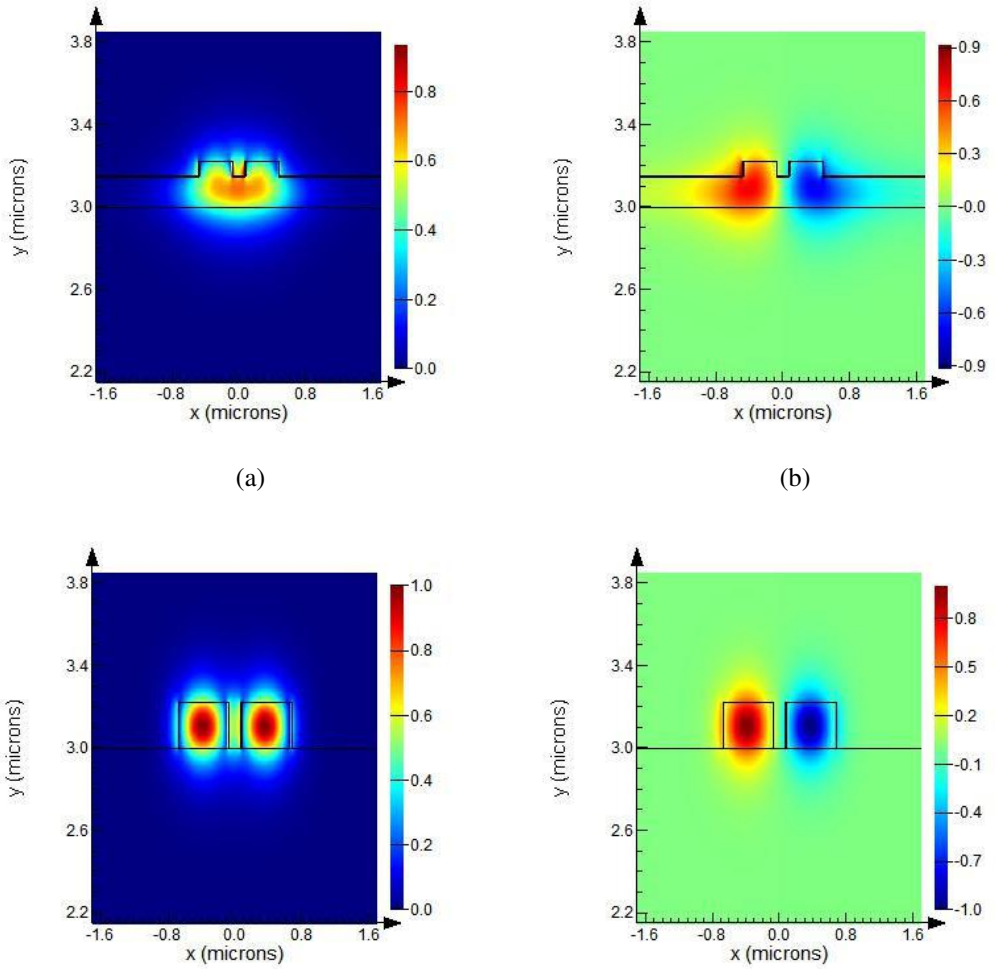

(a) (b)

(c) (d)

Figure 3.1: Mode profiles: (a) Shallow etched, symmetric mode (b) Shallow etched anti-symmetric mode (c) Fully etched symmetric mode (d) Fully etched anti-symmetric mode

the field and background refractive index are higher in this case and the interaction area is larger compared to the shallow etched case. So by intuition we can say that the sensitivity will be higher for deeply etched case.

The power transfer between the waveguides in a directional coupler is given in Figure 3.2. The mode profile is obtained by 2.5 FDTD method using Lumerical Mode solver. We can see that the total power is oscillating between the waveguides of the directional coupler with distance. The cross coupling length (L_c) of the directional coupler in this case is about 45 μm.

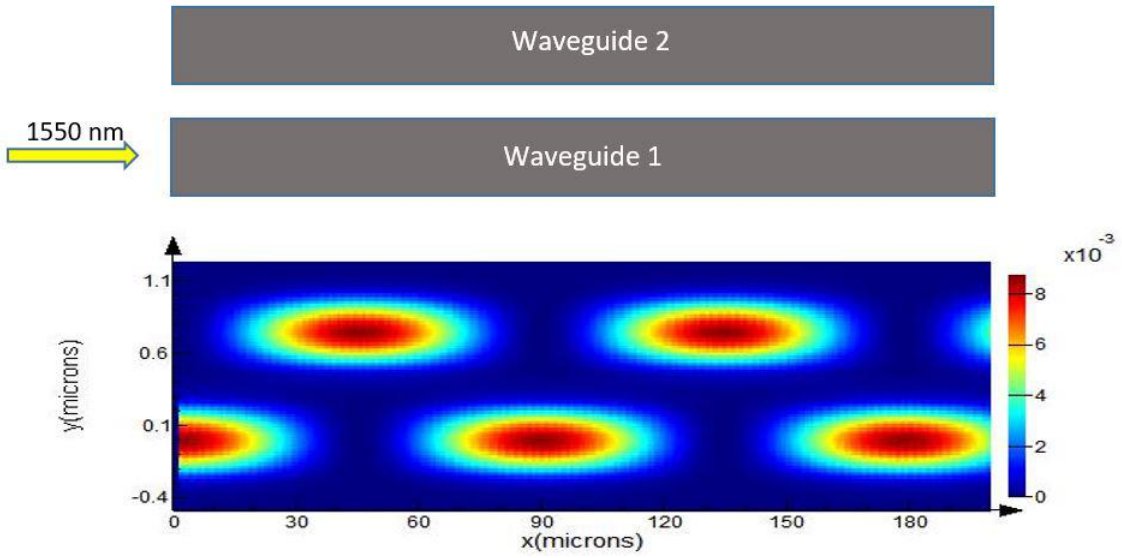

Figure 3.2: Power transfer in a directional coupler (Generated using 2.5 FDTD 3D profile monitor)

3.1.2 Confinement and bending Losses

The loss in the waveguide plays an important role in the performance of ring resonator based device. Losses can decrease the Quality factor of the resonator and which in turn decrease the limit of detection of the sensor. Since the light inside a resonator travels through it several times (round trips), lossy waveguides will always create problems for longer ring sensor designs. Utmost care should be given while designing bending regions since bending losses can add more problems. Hence it is very important to control bending losses by designing waveguides with highly confined modes. The mode profiles given in Figure 3.3 and 3.4 ,for different waveguide dimensions gives an idea about confinement and losses.

In shallow etched waveguide a large amount of the power is propagating through the slab region and it is spread over it. We can see that the mode is tightly confined inside fully etched waveguide compared to shallow etched one. The mode profiles given in Figure 3.4 represents profiles for bend waveguides for both the above mentioned dimensions for a bend radius of 25 micro meter. It shallow etched case, we can see a shift in mode to the right side of the waveguide due to the bending, but that shift is negligible in the case od deeply etched waveguide (Figure 3.4).

We calculated the bending losses in each case using metal boundary conditions in

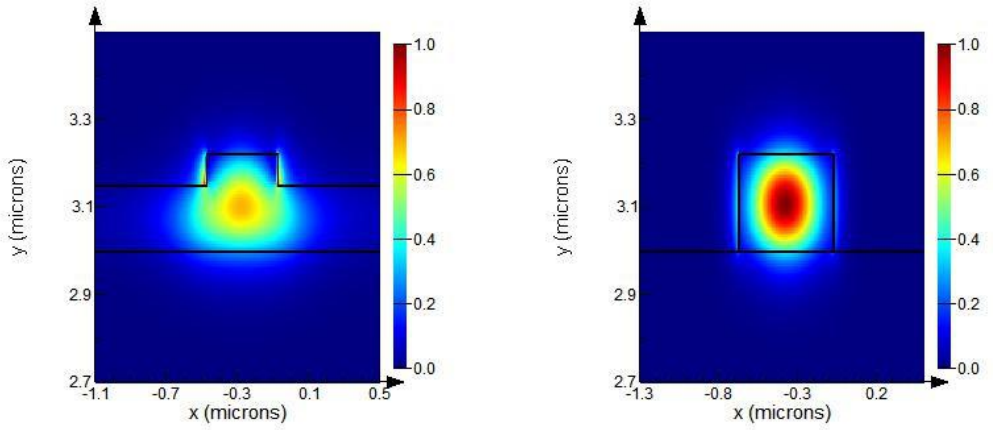

(a) (b)

Figure 3.3: Mode profiles of waveguides: (a) Shallow etched (b) Fully etched

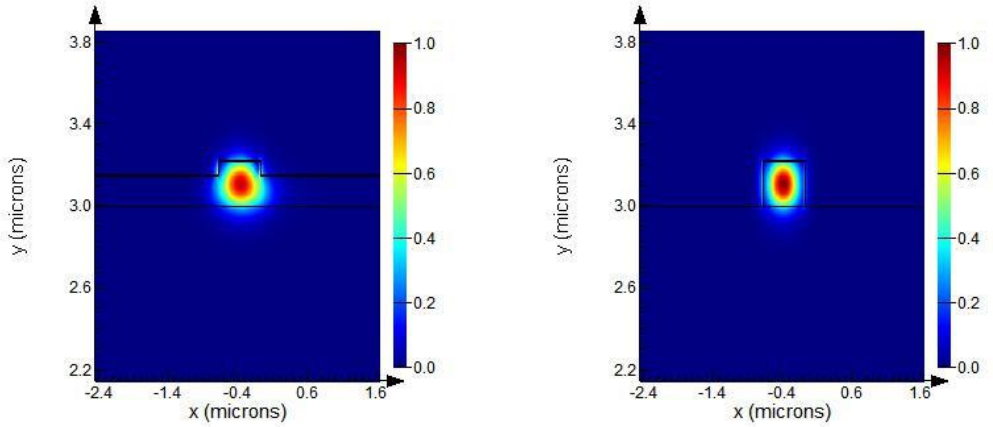

(a) (b)

Figure 3.4: Bend waveguide Mode profiles: (a) Shallow etched (b) Fully etched

Lumerical Mode solver. In shallow etched case the loss is about 3.5 dB/cm and in the case of fully etched bend waveguide the loss is nearly 0.5 dB/cm. So fully etched waveguides are more promising in the case of losses and confinement of power. The map of waveguide confinement factor for different waveguide dimensions is given in Figure 3.5.

From the plot it is evident that the confinement is higher for deeply etched waveguides. About 85 % of the total power is confined in the waveguide region for fully etched waveguide of width around 550 nm. In shallow etched waveguides, the mode is distributed in waveguide as well as slab region. So the power confinement in the

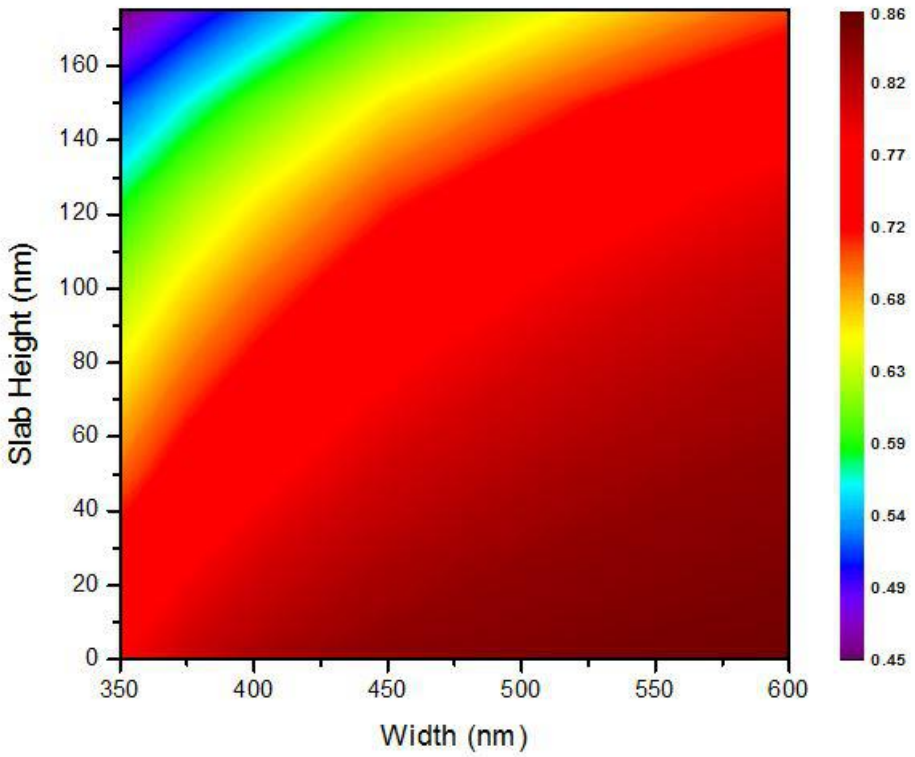

Figure 3.5: Power confinement map

waveguide region is lower (below 50 percentage) as expected.

It is important to have a better confinement especially in the case longer devices to reduce the overall loss. Since the light in a ring resonator travels so many round trips inside the ring, loss is a very important parameter which should be taken care in device design. So, deeply etched waveguides with 85% power confinement are suitable for our sensor design.

3.1.3 Sensitivity maps

We already discussed about the importance of directional coupler dimensions on the sensitivity of a critically coupled device. The interaction of evanescent field with the background refractive index is the main factor in the case of sensitivity. We can analyze these things from the following simulation results. The sensitivity map for different directional coupler dimensions are given in Figure 3.6.

Maps shows that the sensitivity is higher for deeply etched directional couplers with

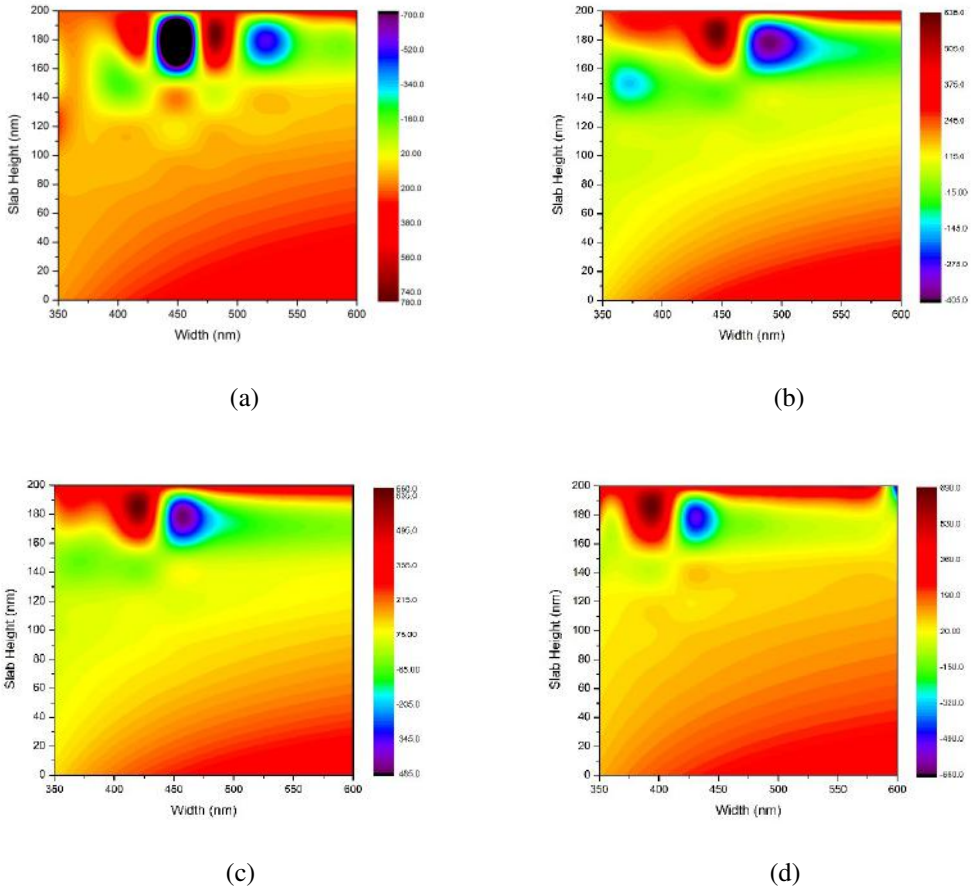

Figure 3.6: Sensitivity maps for different gaps of directional coupler: (a) Gap 50 nm (b) Gap 100 nm (c) Gap 150 nm (d) Gap 200 nm

larger width waveguides (about 600 nm). The maps for different gaps follows almost the same pattern, but the sensitivity varies slightly for different gaps. The increase in sensitivity for deeply etched wide waveguide directional couplers can be justified by the increased interaction area of the background refractive index with the electric field. There are certain regions in the map which shows insensitive areas as well as negative sensitive areas. Negative sensitivity means that the shift in critically coupled wavelength will be to higher wavelength side of the spectrum (Red shift). The insensitivity regions in the maps needs further investigations to explain the physics behind it. Since it is beyond the scope of this work, we are leaving that for further investigations later. Another important parameter which plays a role in sensitivity is the gap of the directional coupler. The change in sensitivity with the directional coupler gap is given in Figure 3.7.

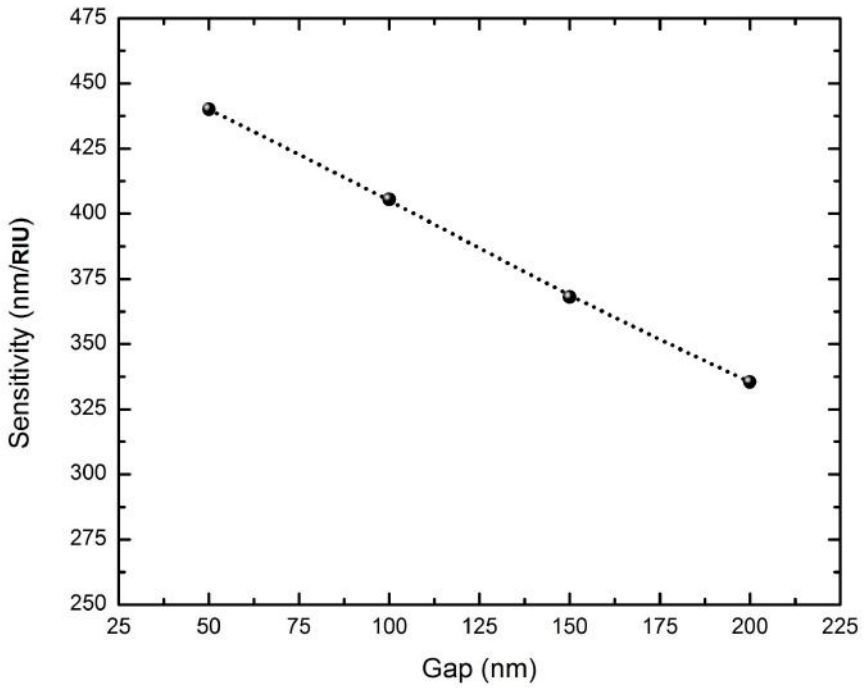

Figure 3.7: Maximum Sensitivity : Directional coupler gap Vs Sensitivity

The plot is for deeply etched (25 nm slab) directional coupler with wider waveguides (550 nm). The behavior of the plot is almost linear and the sensitivity decreases with increase in gap. When the coupler gap changes from 200 nm to 50 nm, the increase in sensitivity is about 100 nm/RIU. Directional coupler with smaller gap will be having mode profiles whose intensity is comparatively higher in the gap region. So, the interaction between background refractive index with the electric field will be increased.

3.1.4 FSR of the ring and Limit of detection (LOD)

In the previous chapter we mentioned that the Limit of Detection (LOD) is a measure of accuracy of our sensing device. Free Spectral Range (FSR) plays a major role in limit of detection. If the peaks of a resonator are widely spaced, probability for falling the critically coupled wavelength exactly in the resonance dips is very less. And if the resonance dips are very closely spaced, the probability is high and limit of detection will be improved.

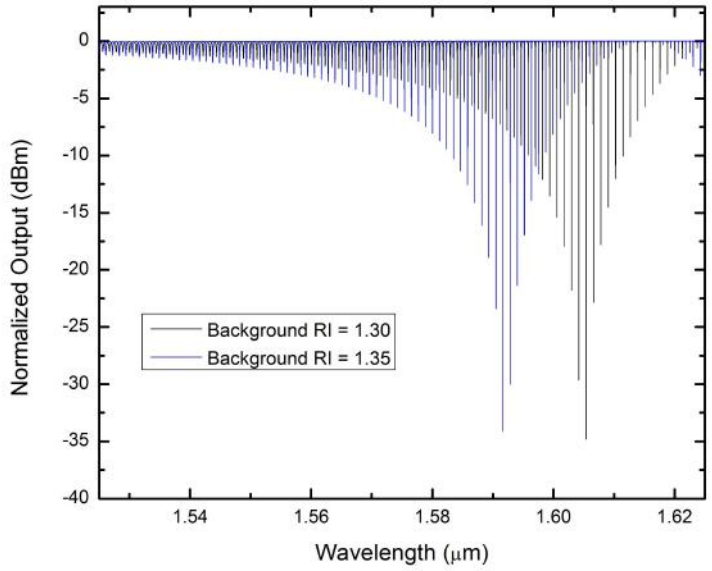

(a)

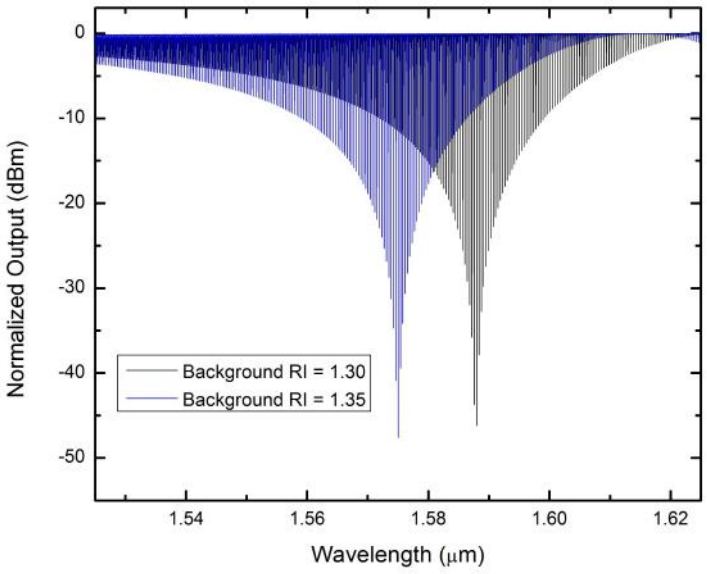

(b)

Figure 3.8: Simulated output spectra of critically coupled ring resonator sensor for two different background refractive indices: (a) Ring with perimeter about 0.5 mm (b) Ring with perimeter about 1.5 mm

The plots are simulated output spectra for critically coupled ring resonator for two different rings. Each plot have two different spectra for background RI values 1.3 (Black) and 1.35 (Blue). The first plot is for smaller ring and second one is for larger

ring. Comparing the plots it is clear that the FSR of the larger ring is lower and that increases the accuracy of the measurement of shift in resonant wavelength.

3.1.5 Designs for high Sensitivity and Limit of Detection

We have discussed about Sensitivity and limit of detection of a sensor and how we can control these by proper design of directional coupler and ring dimensions in a device. From the simulation results it is clear that the deeply etched and larger width waveguide directional couplers are more sensitive. Also we have been seen that the Q-factor and the FSR of the resonator plays a major role in limit of detection of a sensor. Deeply etched waveguides with low loss and larger perimeter rings are suitable for our requirement. The dimensions of the directional coupler designed for higher sensitivity is given in Figure 3.9.

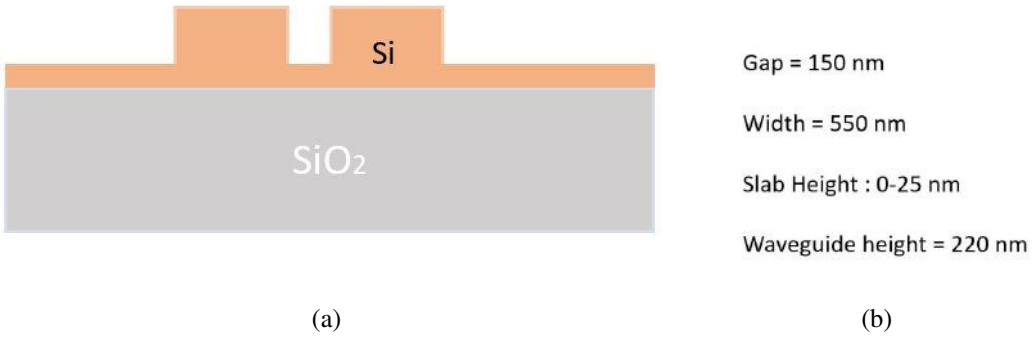

(a) (b)

Figure 3.9: Cross sectional view of directional coupler design in 220 nm device layer thickness.

We have considered the fabrication possibilities while designing the directional coupler. A slab of less than 25 nm thickness is kept in the design for tuning purposes (like integrating heater for wavelength tuning). direction coupler gap is chosen 150 nm for avoiding resolution of fabrication steps.

Compact device designs

Our ultimate aim is to integrate the sensor in a chip and for that we need compact devices. Since our ring resonator should be larger for better LOD, we should be careful

in designing larger rings in smaller area for keeping the device compact. The design given in Figure 3.10 will be suitable for a compact device. In this design we can increase the perimeter of our ring as much as we want by stretching the ring in the horizontal direction parallel to the straight waveguide.

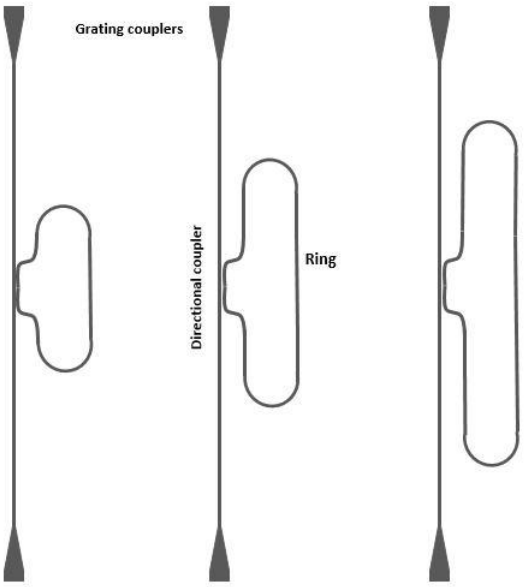

Figure 3.10: Compact design for ring resonator sensor for rings with different perimeters keeping the other components in design identical.

Since the input to output grating coupler distance is about 5 mm, we can increase the size of the ring in the horizontal direction ring perimeter more than 10 mm and that is sufficient for obtaining an FSR value needed for achieving a better limit of detection. The component given in both ends of the straight waveguide is called grating coupler which is used for coupling light back and forth between our device and optical fiber.

Grating Coupler design for 220 nm device layer

One important component in our sensor design is Grating coupler and tapering region used for light coupling from the fiber to the input of our waveguide and from the output of waveguide to the fiber connected to the optical spectrum analyzer. The periodicity required for a grating coupler bandwidth peak at 1550 nm in 220 nm silicon layer with etching of 90 nm is calculated as 640 nm. The duty cycle is set to be 50 percentage.

The grating coupler is designed for 10^o coupling angle between fiber and line per-

Figure 3.11: Grating coupler in 220 nm SOI : Side view

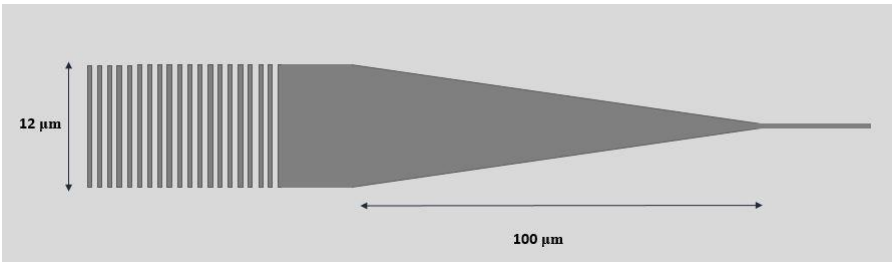

Figure 3.12: Grating coupler with taper region : Top view

pendicular to the grating direction. The grating region is around $12 \times 12\mu m^2$ wide. An extra tapering region of 100 μm is included between input waveguide and grating coupler for maintaining single mode condition while coupling light into the waveguide.

Output spectra and FSR

Since the directional coupler dimensions are same, the calculated sensitivity is around 260 nm/RIU for all designs. The FSR of the rings varies from 500 pm to 80 pm as the ring length increases from 1 mm to 7 mm. The simulated spectra for three different rings and their corresponding FSR are plotted given in the Figure 3.13.

Each plot contains spectra for two different background refractive index values. The shift in critically coupled wavelength is 13 nm for 0.05 RIU change, hence the sensitivity is 260 nm/RIU for all cases. The decrease in FSR with increase in ring length is evident from the spectra. The biggest ring is 7.195 mm long and it has the least value of FSR about 90 pm. The FSR values of different rings for two different slab heights are tabulated and plotted in Figure 3.14.

The FSR of a resonator is inversely proportional to the ring length, so the behavior of graph is expected. Since the group index n_g is different for different slab heights, the FSR values are slightly different in each case. Deeply etched waveguides have higher

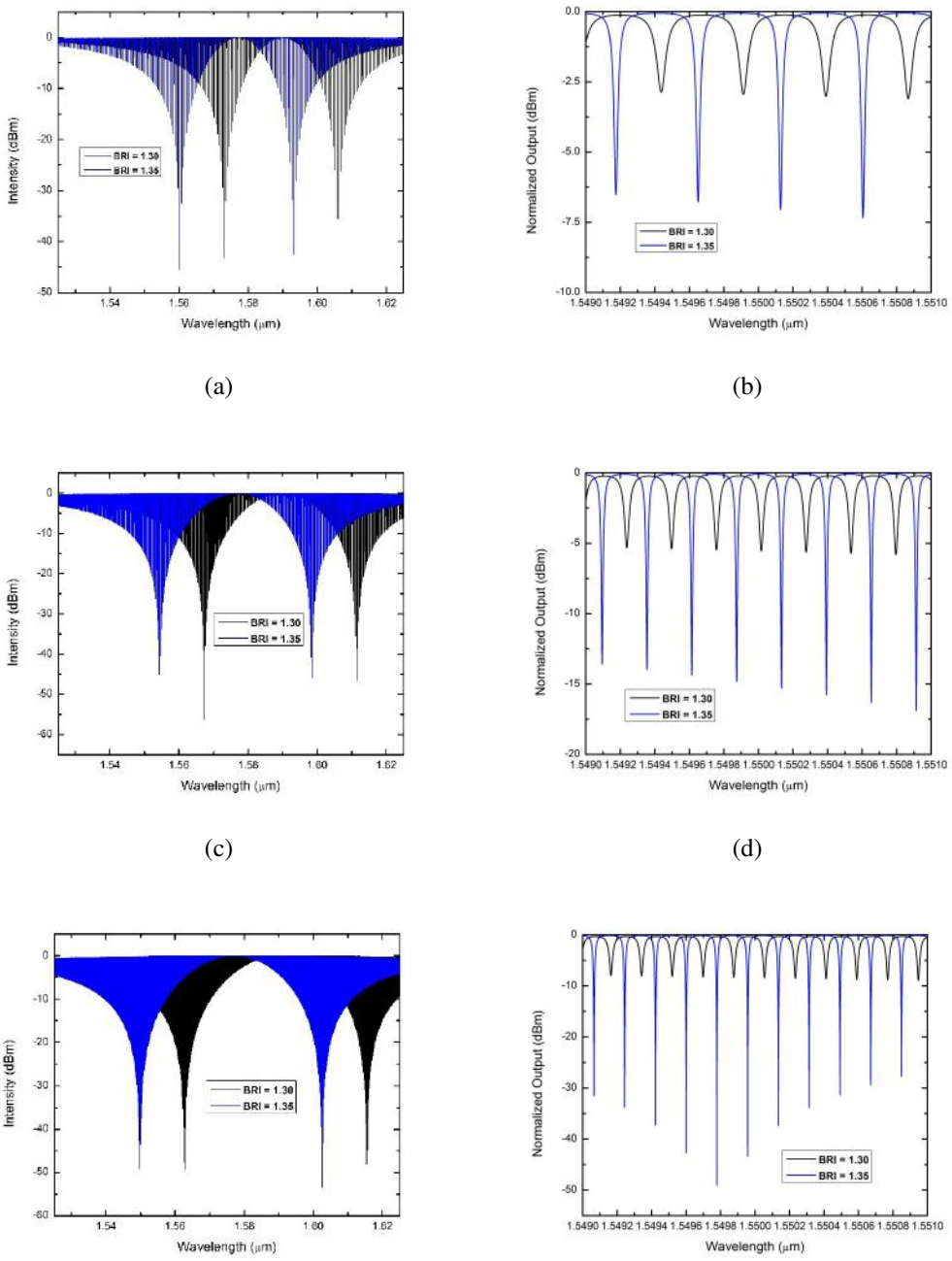

Figure 3.13: Simulated Output spectra and FSR of ring resonators for two different background indices : (a) and (b) Ring perimeter 1.195 mm , (c) and (d)Ring perimeter of 2.195 , (e) and (f) Ring perimeter of 3.195 mm

n_g comparing with shallow etched waveguides, and hence the FSR is slightly lesser for deeper etching.

Ring Length (μm)	Free Spectral Range (FSR)(pm)	
	Slab height 125 nm	Slab height 25 nm
1195	**519.5**	**474.2**
2195	**282.8**	**258.2**
3195	**194.3**	**177.4**
4195	**148**	**135.1**
5195	**119.5**	**109.1**
6195	**100.2**	**91.47**
7195	**86.28**	**78.76**

Figure 3.14: Ring perimeter Vs FSR

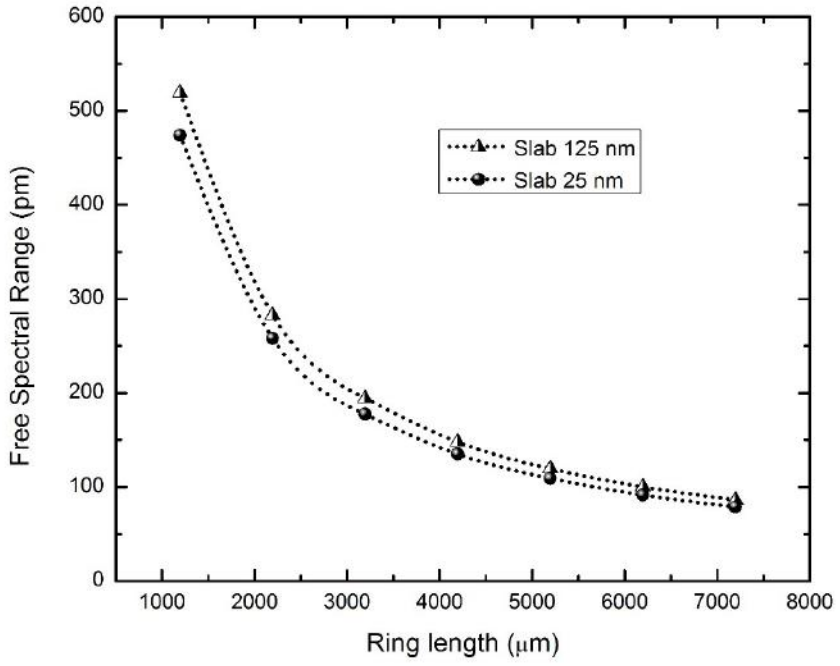

Figure 3.15: Bio-sensing technique using micro-ring resonator

Uniformity in Sensitivity

Another important property of refractive index sensor is the uniformity in the sensitivity for a range of refractive index values of different analytes. We studied variation in

sensitivity for deeply etched case (25 nm slab) with change in background refractive index values ranging from 1 to 1.8 and the behavior is plotted in Figure 3.16

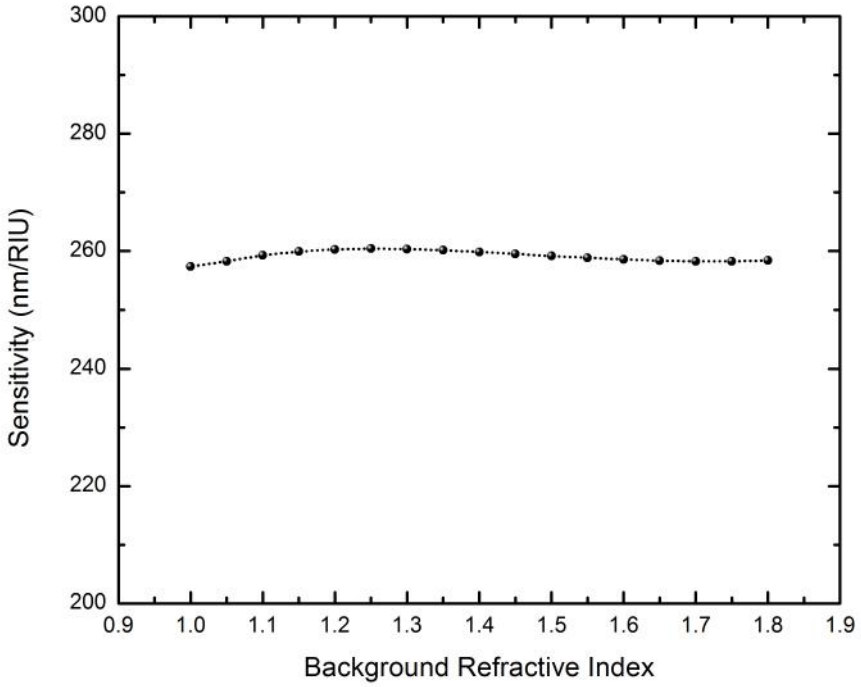

Figure 3.16: Background Refractive Index Vs Sensitivity

The plot shows a uniform behavior in sensitivity for wide range of cladding refractive index. The average value of sensitivity is about 260 nm/RIU and the variation in sensitivity in the refractive index range 1 to 1.8 is only less than 5 nm. So, our design promises a very good behavior in wide range uniform refractive index sensing.

Increased Limit of Detection (LOD)

We could see that the FSR of the ring can be increased by increasing the perimeter of the ring. In our design we have obtained an FSR about 80 pm for a ring length of 7.195 mm. It means that even a change of less than 100 pm in critically coupled wavelength can be obtained and hence the resolving power of the device can be increased. Since the sensitivity is higher (260 nm/RIU), we can measure a change of 0.0003 RIU change of cladding index. So, LOD of the proposed device can be « 10^{-4} RIU.

3.2 Fabrication and Characterization

Fabrication involves patterning in SOI and etching the pattern for desired depth followed by cleaning of resist from the sample. Since our designs are having dimensions around 500 nm, we have to use Electron Beam Lithography for fabrication. For etching we will use Inductively Coupled Plasma Reactive Ion Etching machine (ICPRIE). Our designs contains mainly a grating coupler region and a ring resonator region and the etch depths for both are not same. Since we need light coupling in a wider bandwidth, the grating coupler should be shallow etched about 90nm. The ring resonator region should be etched more than 200 nm for high sensitivity. So, total fabrication process will involve 2 step etching.

3.2.1 Spin coating and Electron Beam Lithography

Lithography process involves coating an electron beam resist uniformly over the sample and patterning it using optimized dose of electron beam. There are two type of resists, positive e-beam resist and negative e-beam resist. We will be using a negative e-beam resist named HSQ. The HSQ is coated in the sample using spin coating machine. The thickness of the HSQ is very important for our patterning process and etching process, and it may change according to the parameters used for spin coating. The thickness is controlled by mainly by the acceleration of the spin coating system. The dependence of acceleration on HSQ thickness is studied by imaging the cross section of sample by scanning electron microscopy (SEM). Some of the images are given in Figure 3.17.

The measured values of thickness for different acceleration is plotted and given in Figure 3.18.

The thickness of the film is exponentially decreasing with increase in acceleration of spin coating and it almost saturates around 100 nm. The maximum speed and time of spin coating is kept as 2500 rpm and 60 seconds respectively. For etching higher depths, we need thicker coatings if the selectivity of the resist is poor. From the results, we can conclude that lower spinning acceleration can give thicker resist coatings.

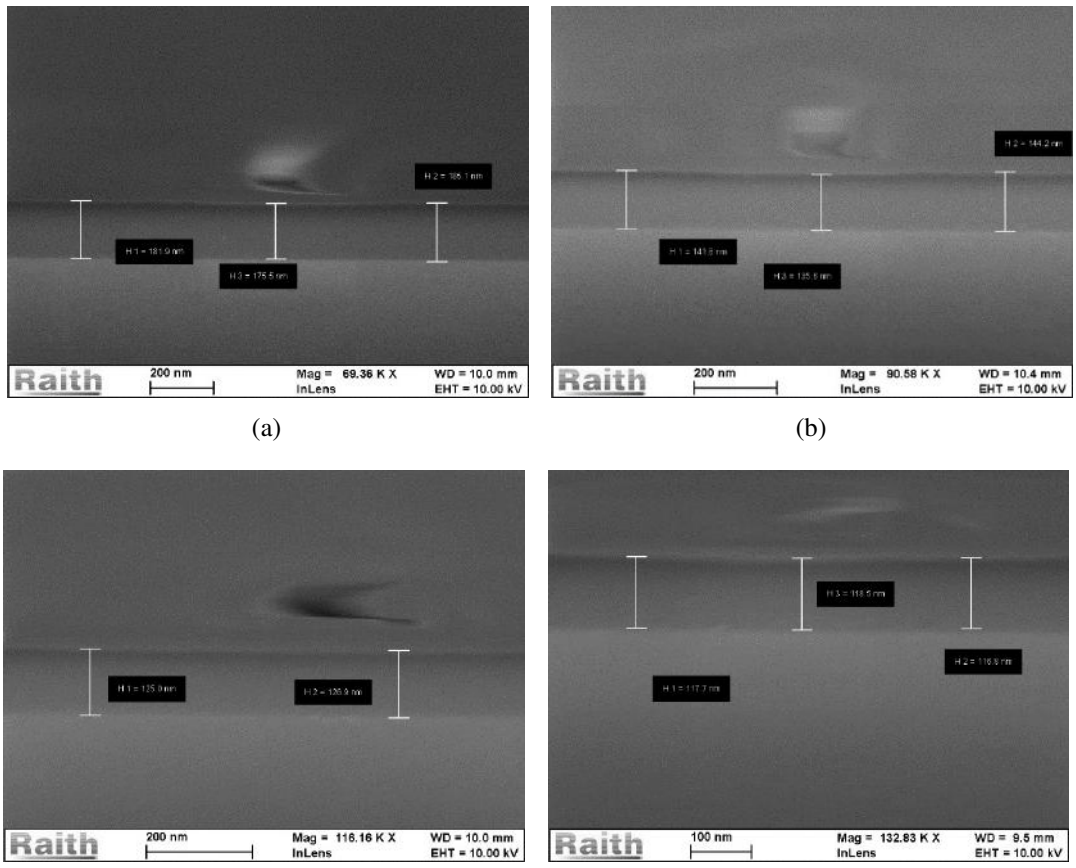

Figure 3.17: SEM images of HSQ coating on silicon for different spin coating accelerations

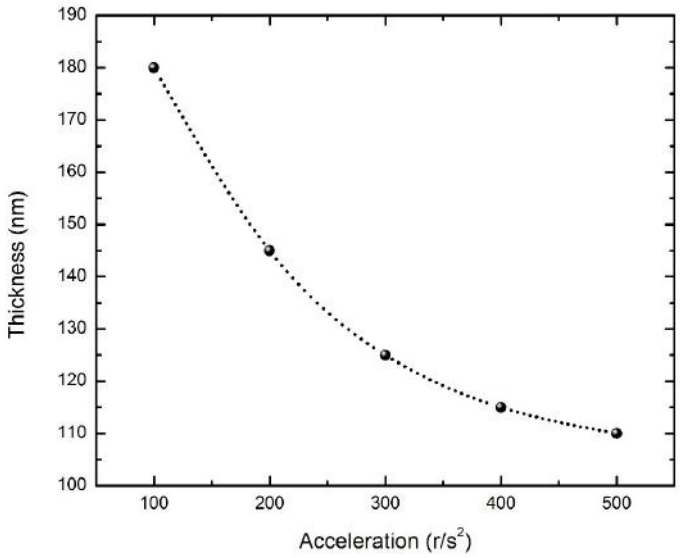

Figure 3.18: Spin coating acceleration Vs Thickness of HSQ coating

3.2.2 ICPRIE etching rate and Selectivity

Next step is to study the selectivity and etching rate of ICPRIE etching process for HSQ coated silicon substrate. For that we coated a bulk silicon sample with 100-120 nm HSQ and patterned it using e-beam lithography system. And the samples are etched using ICPRIE for different etching time keeping other parameters same. The etching parameters used are: Temp 20^o C, RF power 30 Watt, ICP 1000 Watt, Pressure 15 mT and the flow rate of gases were $SF_6 : CHF_3 = 5 : 18$ sccm. All these parameters are kept constant except the etching time for different samples. Some of the SEM images after etching is given in Figure 3.19.

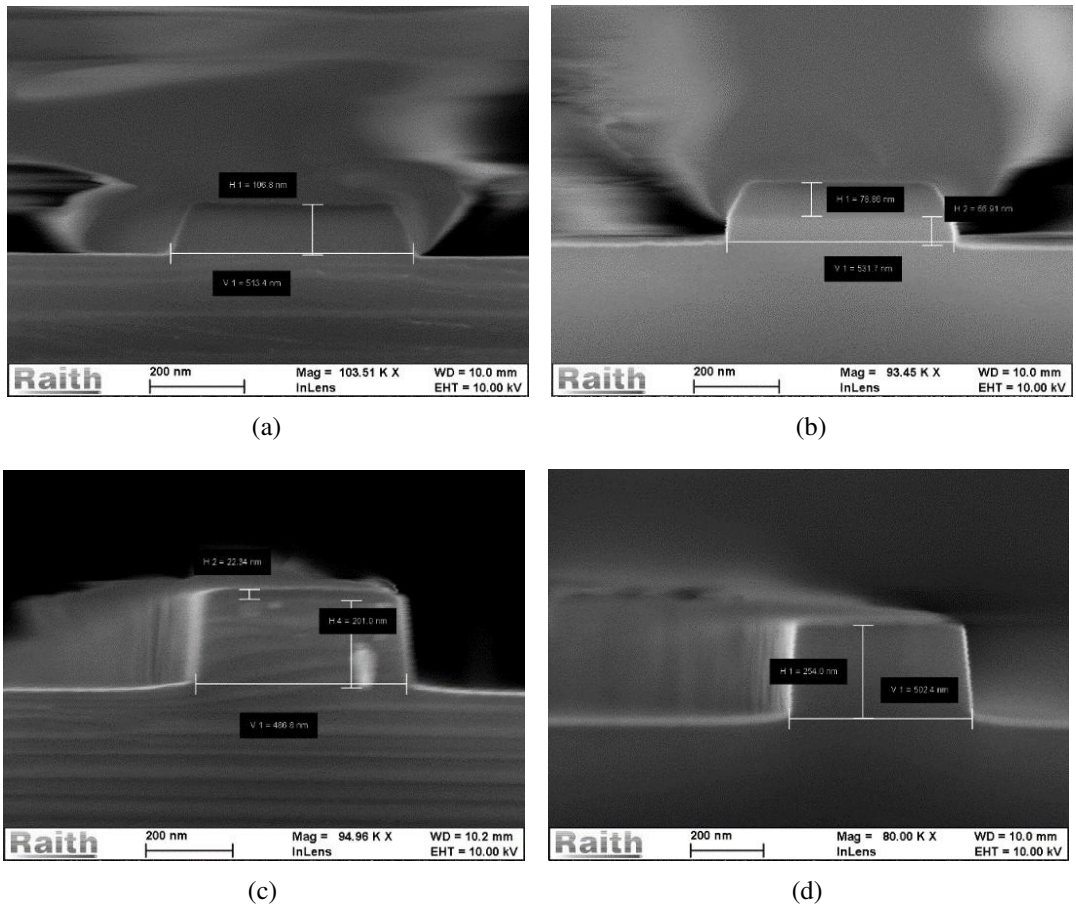

Figure 3.19: SEM images of silicon samples etched for different etching time duration

In the given images, the first one is the patterned HSQ coating before etching and the thickness is about 105 nm. The remaining images are of different etching time. Since the walls of the etched samples are almost vertical we can say that the slope in the side walls of HSQ will nor effect the verticality of etched samples. The etching

depth versus time for both the Silicon and HSQ is given in the Figure 3.20.

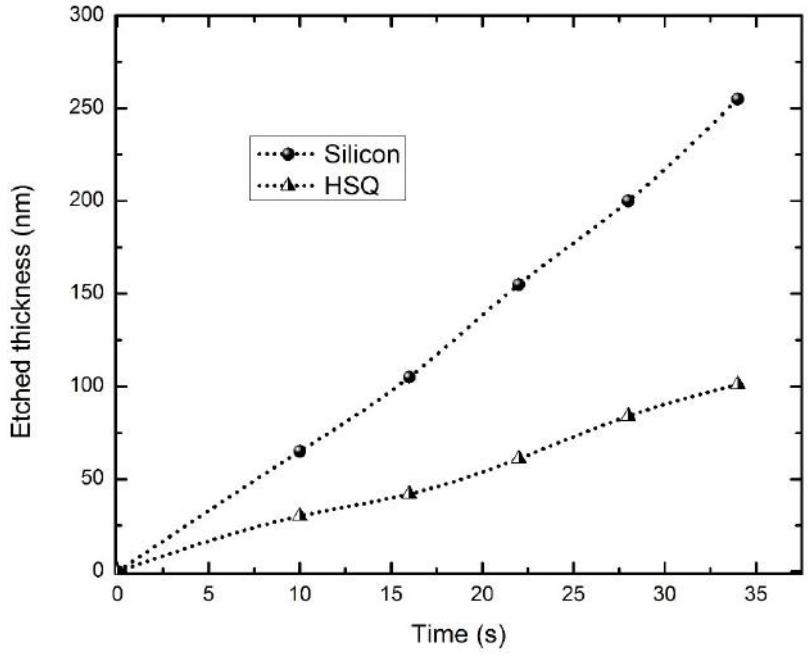

Figure 3.20: Etch depth for silicon and HSQ with time

The behavior of graph is almost linear. The etching rate of silicon is higher and it is found to be about 7 nm/s and the selectivity of etching Silicon : HSQ is 5 : 2. So we can etch about 250 nm silicon with a 100 nm thick HSQ. Since we are using 220 nm device layer SOI for fabricating the device, 100 nm HSQ is sufficient for fabricating a deeply etched device. For 200 nm etching the time required is 28 seconds.

3.2.3 Mask layout for compact devices

For fabricating the device we need a mask to pattern the design in SOI using electron beam lithography. We designed mask with one set containing seven rings whose perimeter ranges from 1.195 mm to 7.195 mm for fabrication as given in Figure 3.21 and 3.22. We can see that several devices can be placed in smaller area if we are using this type of horizontally stretched ring resonator design.

The mask layout is designed such a way that there is no coupling between ring and the straight waveguide except in the coupler region. The bending radius of decoupling

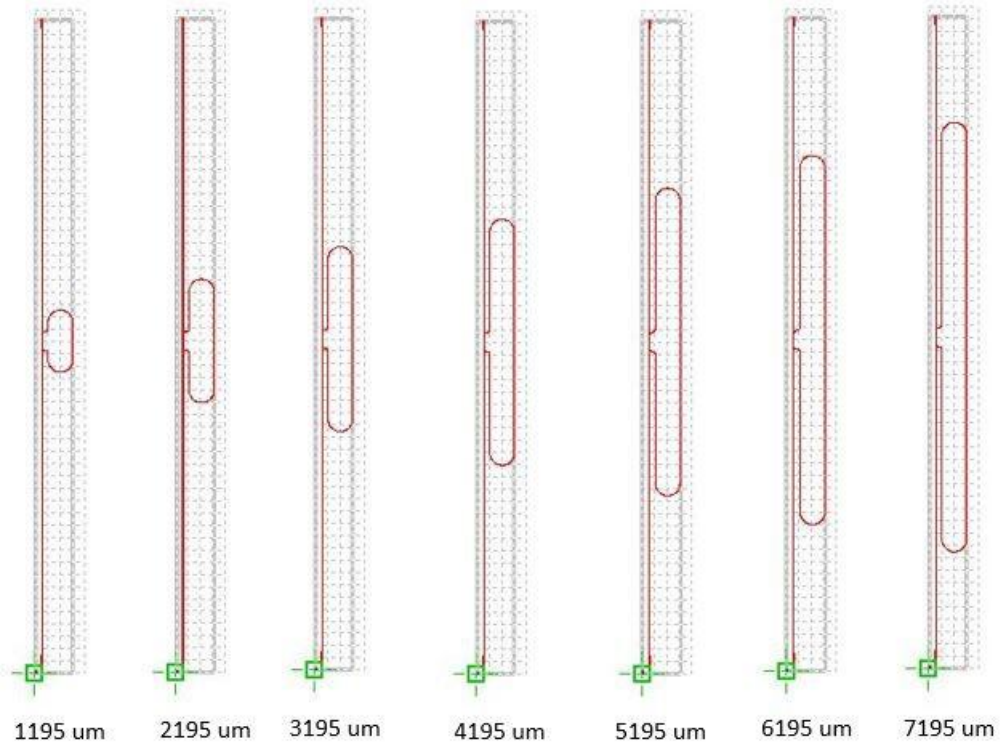

Figure 3.21: Mask layout designed for fabrication : rings with different perimeter

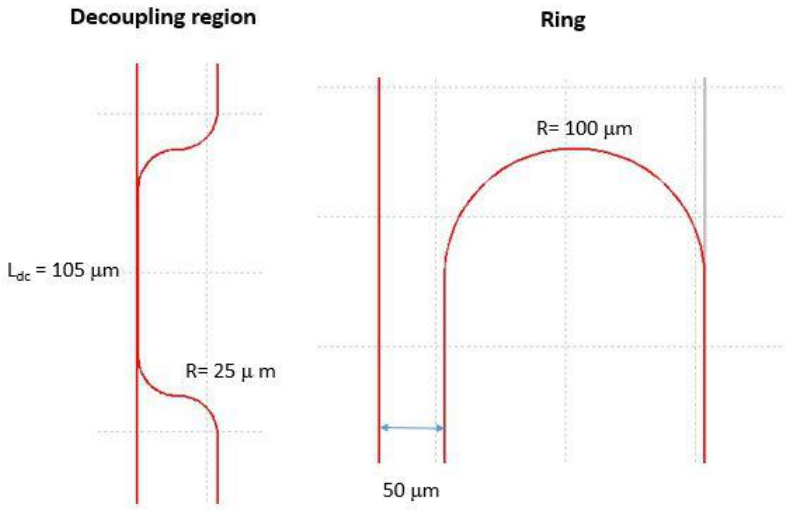

Figure 3.22: Zoomed view of mask layout designed for fabrication : directional Coupler and ring.

region is kept 25 μm to avoid bending losses. And the ring radius is kept 100 μm which is sufficient to get almost lossless bending.

3.2.4 Patterning and Etching

Next step is to pattern our original device in SOI using Electron Beam Lithography. The total device contains several individual components which need different type of patterning strategy and electron beam dose. Since I don't have much experience in fabricating whole device in SOI, my lab mate and PhD scholar Ramesh Krishnan agreed to fabricate it for me. After patterning, he etched the sample about 90 nm to obtain the required etch depth for grating coupler as first step. The SEM image of the directional coupler region is given in Figure 3.23.

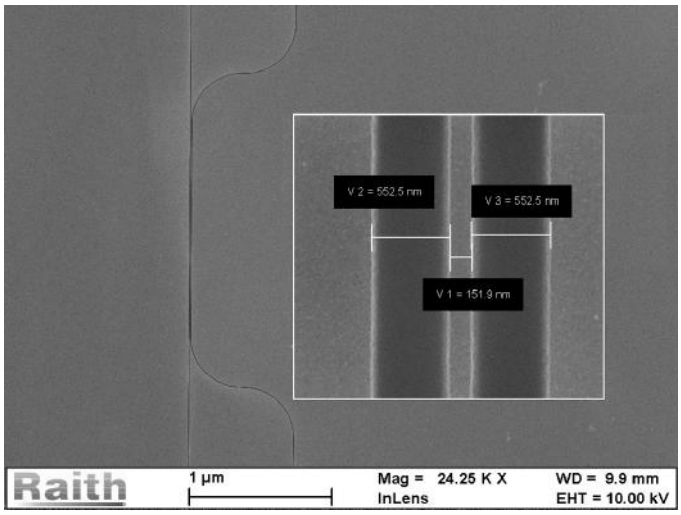

Figure 3.23: The top view SEM image of the directional coupler after patterning

Output spectra and FSR values after first step of etching

The etching step required for grating couplers are done using ICPRIE etching for an etching depth of about 90 nm. We characterized the devices using optical spectrum analyzer. Some sample output spectra are given in Figure 3.24 and 3.25. The directional coupler length was 105 μm.

The plots are for ring perimeters from 1.195 mm to 7.195 mm. The zoomed spectra are also given to show the change in FSR. We can clearly see that the peaks are closely spaced for larger rings. The experimentally obtained values from the fabricated devices and simulated values of FSR for different devices with 125 nm slab region are plotted in Figure 3.26. Both curves follows almost same path and experimentally obtained values well matches with the simulated results especially in the case of longer rings.

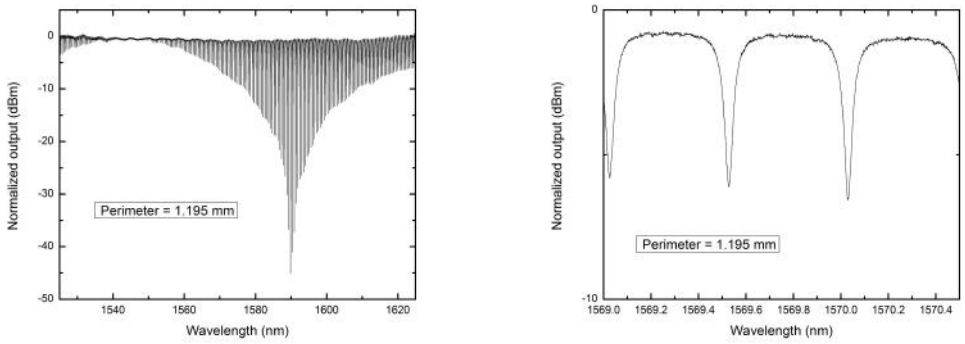

(a) (b)

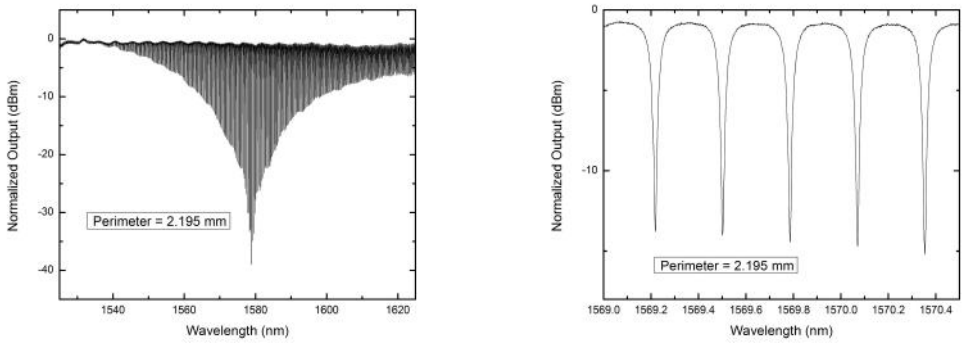

(c) (d)

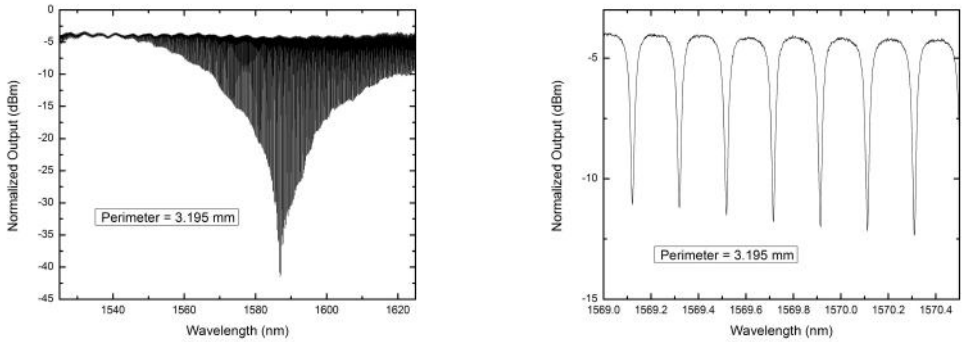

(e) (f)

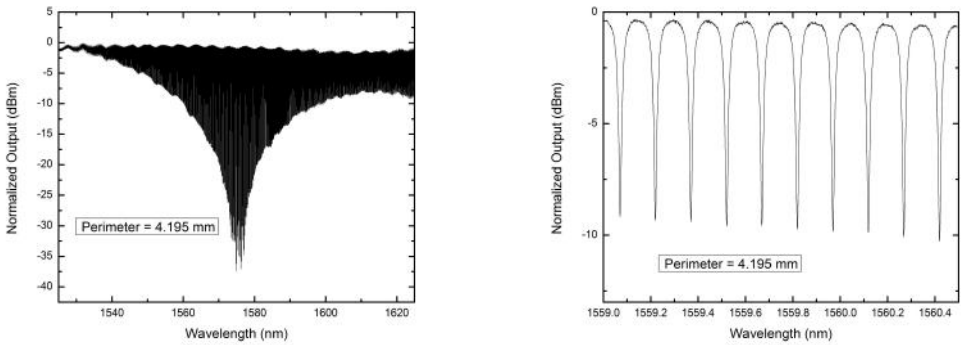

(g) (h)

Figure 3.24: Output spectra and zoomed view of the plots for fabricated rings with different perimeter

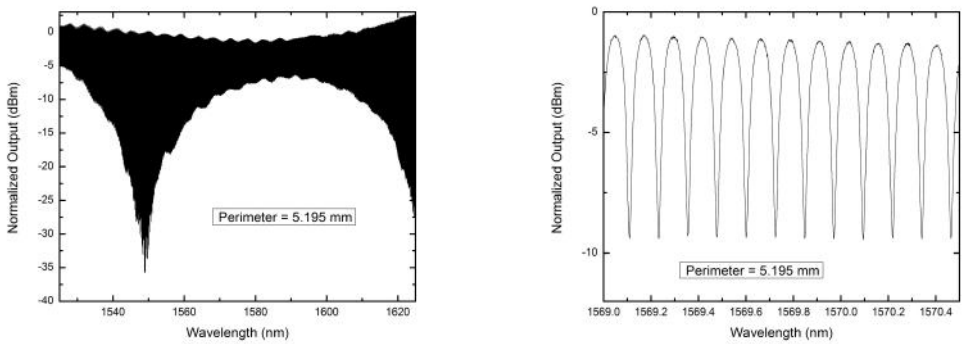

(a)

(b)

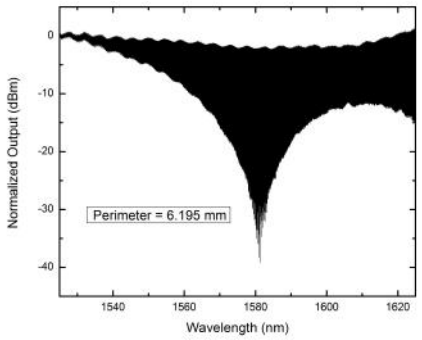

(c)

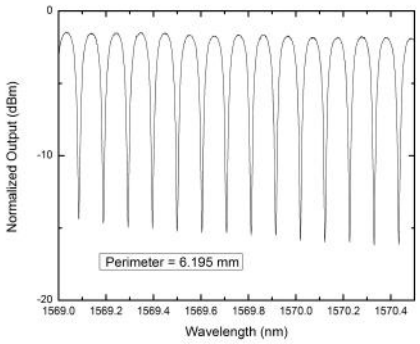

(d)

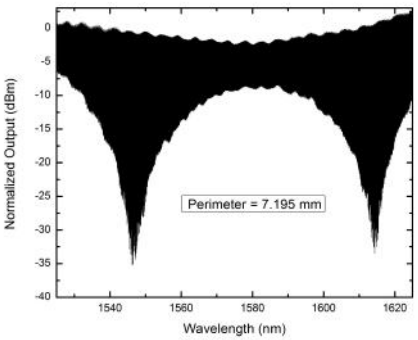

(e)

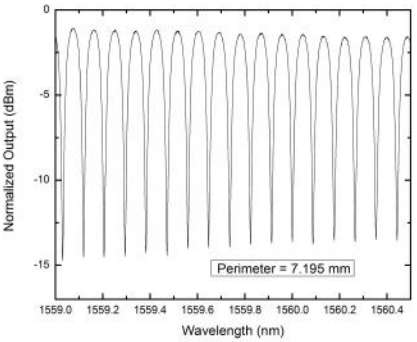

(f)

Figure 3.25: Output spectra and zoomed view of the plots for fabricated rings with different perimeter

Quality factor

Another important parameter of a resonator is Quality factor, which is the ratio between average energy stored in the resonator to the total energy dissipated in a cycle. The change in quality factor with ring perimeter is plotted in figure 3.27.

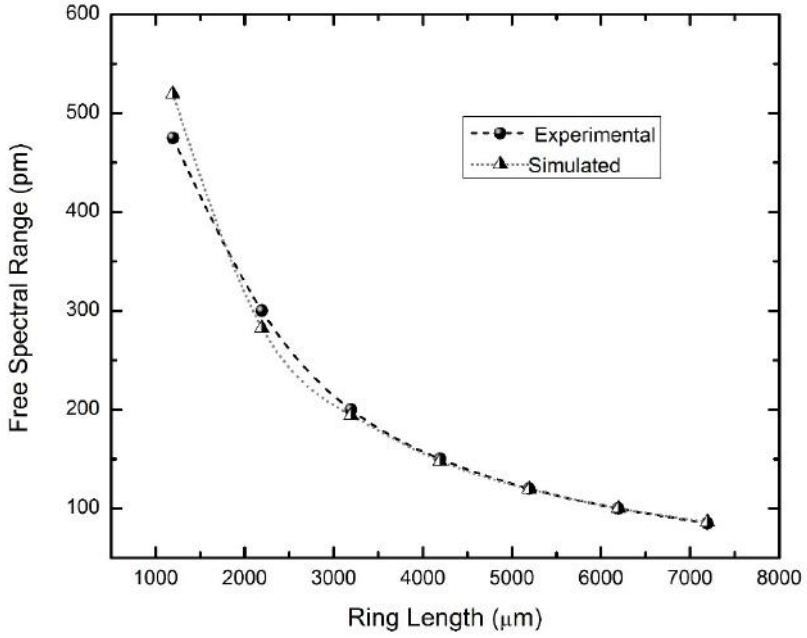

Figure 3.26: Ring perimeter Vs FSR : Comparison between simulated and fabricated devices(for 90 nm etch depth)

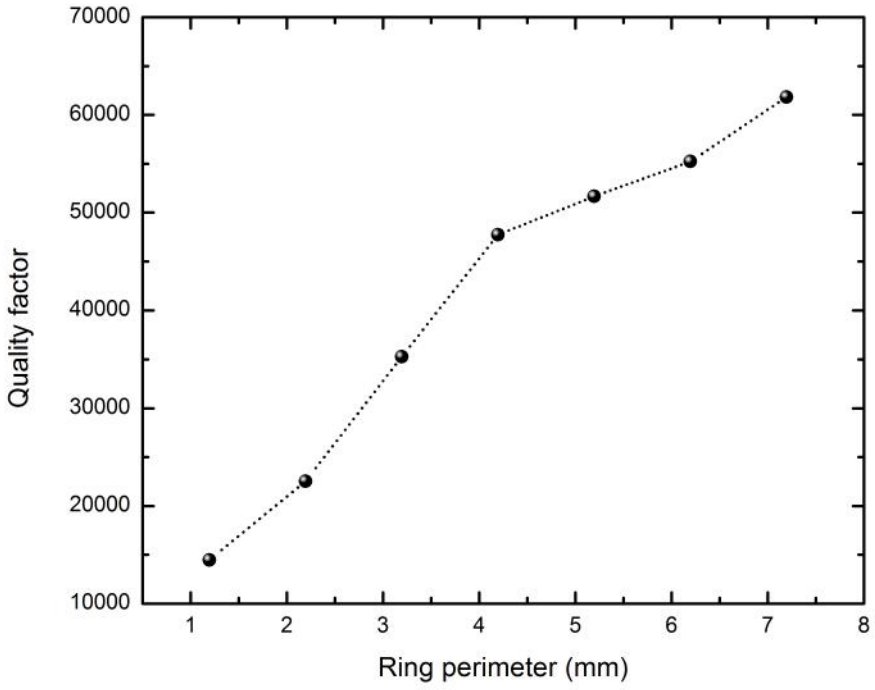

Figure 3.27: Ring perimeter Vs Q-factor

The Q-factor varies from about 15000 to 61000 as the ring perimeter increases. The average energy stored in a resonator is proportional to the total volume of the resonator. Rings with larger perimeter have larger volume, and hence the Q-factor is very high for larger rings as expected. Resonator devices with higher Q-factors have better limit of detection (LOD).

Sensitivity

After the first part of etching (90nm), we calculated the sensitivity of the device by putting water (n=1.33) in the directional coupler region. The output spectra recorded with OSA is given in Figure 3.28.

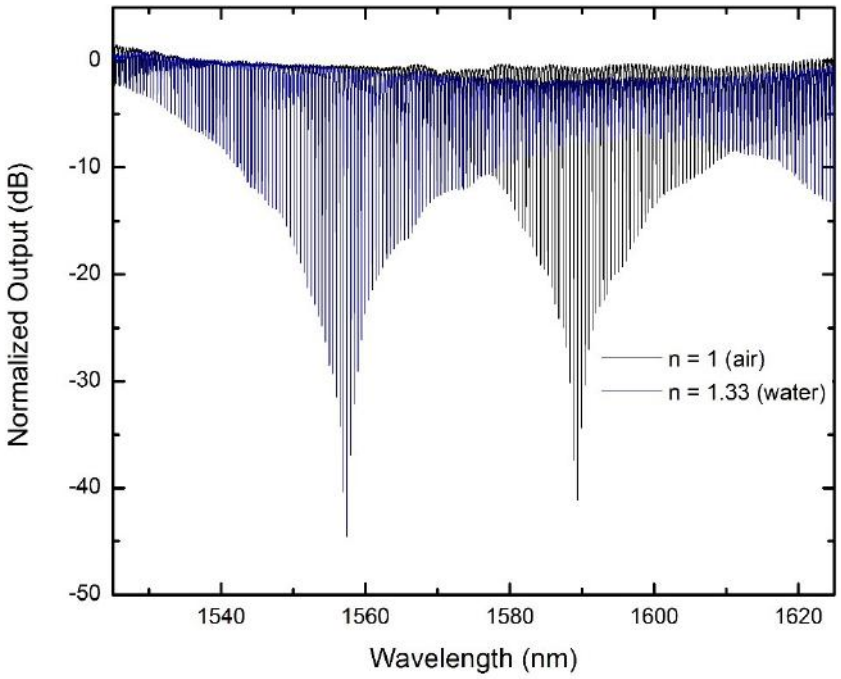

Figure 3.28: Output OSA spectra of fabricated device(after 90 nm etching) for two different cladding refractive indices.

The black colored spectra stands for air as cladding and blue colored spectra stands for water as cladding. The observed blue shift in wavelength was 31 nm and then the average sensitivity of the device is about 95 nm/RIU. The sensitivity obtained from simulation results was about 80 nm/RIU. The slight change may be due to the variations in

expected etch depth or directional coupler gap during fabrication process. Also simulation results have been done for closely spaced refractive index points (1.3 and 1.35). But in characterization we are getting an average sensitivity for the range 1 to 1.33 RIU. The lower FSR of the ring help us to identify the critically coupled wavelength accurately.

CHAPTER 4

Conclusion

4.1 Summary

Computational analysis for critically coupled ring resonator based refractive index sensors shows that the sensitivity can be increased by controlling the direction coupler dimensions of the device. Deeply etched directional couplers (25 nm slab) with wider waveguides (550 m) are more sensitive than shallow etched case. The sensitivity obtained from simulation results are 260 nm/RIU for deeply etched directional coupler. The limit of detection (LOD) of the device can be improved by reducing the FSR of the ring. Smaller FSR values about 80 pm is obtained by designing a ring with perimeter about 7 mm. From this we could obtain the limit of detection of the proposed sensor device less than 10^{-4} RIU.

The spin coating parameters have been optimized for getting desired value of HSQ thickness for the fabrication of the proposed device by deep etching more than 200 nm. The ICPRIE etching rate of Silicon and HSQ have been studied and shown that more than 250 nm of silicon can be etched with an HSQ coating of 100 nm. The etching rate of silicon obtained is about 7 nm/s and the selectivity of etching is 5:2 (Si:HSQ). The characterization results of proposed device after first step of etching (90 nm etch depth) well agrees with the simulation results. The sensitivity obtained was 95 nm/RIU and the FSR value obtained for 7.195 mm ring was 80 pm. The Q-factor of the ring varies from 15000 to 61000 as the ring perimeter increases. The maximum Q-factor value obtained is about 61000 for a ring with 7 mm perimeter. The sensitivity can be increased up to 260 nm/RIU by etching the device deeply about 200 nm. The superiority of the proposed integrated optical sensor device lies in its high sensitivity, high Limit of detection, simpler design, easier operation, wider-range of uniform sensitivity.

4.2 Outlook

The proposed device will definitely serve as a good candidate for wide range refractive index sensing with high resolution and sensitivity. The simplicity of design and working principle is the major advantage of the proposed device. A wide range lab-on chip sensor can be developed using the same design by integrating source, detector and active controls (Micro-heater or PIN diodes) in the device for tuning critically coupled wavelength back to resonance. This in fact, can be used for bio-sensing applications and it helps to get rid of the sensing based on spectroscopic measurements where, expensive optical spectrum analyzers are used.

REFERENCES

1. R. R. Schaller "Moore's law: past, present and future", *IEEE spectrum, vol. 34, no. 6, pp. 52-59, 1997.*

2. V. Passaro et al. "Recent advances in integrated photonic sensors", *Sensors, vol. 12, no. 11, pp. 15558-15598, 2012*

3. K. De Vos, I. Bartolozzi, E. Schacht, P. Bienstman, and R. Baets "Siliconon-insulator microring resonator for sensitive and label-free biosensing,", *Opt. Express, vol. 15, no. 12, pp. 7610-7615, 2007*

4. Sujith Chandran, Ramesh K. Gupta, Student Member, IEEE, and Bijoy Krishna Das, Member, IEEE, "Dispersion Enhanced Critically Coupled Ring Resonator for Wide Range Refractive Index Sensing,", *IEEE JOURNAL OF SELECTED TOPICS IN QUANTUM ELECTRONICS, VOL. 23, NO. 2, MARCH/APRIL 2017*

5. R. Guider et al., "Sensitivity and limit of detection of biosensors based on ring resonators,", *Sens. Bio-Sens. Res., vol. 6, pp. 99-102, 2015*

6. G. A. Rodriguez, S. Hu, and S. M. Weiss, Porous silicon ring resonator for compact, high sensitivity biosensing applications,", *Opt. Express, vol. 23, no. 6, pp. 7111-7119, 2015*

7. T. Claes, W. Bogaerts, and P. Bienstman, "Experimental characterization of a silicon photonic biosensor consisting of two cascaded ring resonators based on the vernier-effect and introduction of a curve fitting method for an improved detection limit,", *Opt. Express, vol. 18, no. 22, pp. 22747-22761, 2010*

8. T. Claes et al. "Label-free biosensing with a slot-waveguide-based ring resonator in silicon on insulator,", *IEEE Photon. J., vol. 1, no. 3, pp. 197- 204, Sep. 2009*

9. W. Bogaerts et al. "Silicon microring resonators,", *Laser Photon. Rev., vol. 6, no. 1, pp. 47-73, 2012.*

10. A. Yariv and P. Yeh Photonics: Optical Electronics in Modern Communications (The Oxford Series in Electrical and Computer Engineering)., *London, U.K.: Oxford Univ. Press, 2006.*

11. Goran Z. Mashanovich,* Milan M. MiloÅąeviÄĞ, Milos Nedeljkovic, Nathan Owens, Boqian Xiong, Ee Jin Teo, and Youfang Hu "Low loss silicon waveguides for the mid-infrared", *Advanced Technology Institute, Faculty of Engineering and Physical Sciences, University of Surrey, Guildford, Surrey, GU2 7XH, UK*

12. Antoine Leblanc-Hotte, Jean-Sebastien Delisle, Sylvie Lesage, and Yves-Alain Peter, "The Importance of Single-Mode Behavior in Silicon-On-Insulator Rib Waveguides With Very Large Cross Section for Resonant Sensing Applications", *IEEE JOURNAL OF SELECTED TOPICS IN QUANTUM ELECTRONICS, VOL. 22, NO. 6, NOVEMBER/DECEMBER 2016*

13. Z. Fang and C. Z. Zhao, "Recent progress in silicon photonics: a review," *ISRN Optics, vol. 2012, 2012.*

14. F. Gao, Y. Wang, G. Cao, X. Jia, and F. Zhang, "Improvement of sidewall surface roughness in silicon-on-insulator rib waveguides," *Applied Physics B, vol. 81, no. 5, pp. 691-694, 2005.*

15. F. Gao, Y. Wang, G. Cao, X. Jia, and F. Zhang, "Reduction of sidewall roughness in silicon-on-insulator rib waveguides," *Applied surface science, vol. 252, no. 14, pp. 5071-5075, 2006.*

16. A. Canciamilla, M. Torregiani, C. Ferrari, F. Morichetti, R. De La Rue, A. Samarelli, M. Sorel, and A. Melloni, "Silicon coupled-ring resonator structures for slow light applications: potential, impairments and ultimate limits," *Journal of Optics, vol. 12, no. 10, p. 104008, 2010.*